Polymer Journal, Vol. 38, No. 3, pp. 197–219 (2006)

REVIEW ARTICLES

# On the Development of Naphthalene-Based Sulfonated Polyimide Membranes for Fuel Cell Applications

Yan YIN, Otoo YAMADA, Kazuhiro TANAKA, and Ken-Ichi OKAMOTO†

*Department of Advanced Materials Science & Engineering, Faculty of Engineering, Yamaguchi University, Tokiwadai 2-16-1, Ube 755-8611, Japan*

(Received December 19, 2005; Accepted December 27, 2005; Published March 15, 2006)

ABSTRACT: This article reviews the recent progress made over the past years based on naphthalene-based sulfonated polyimides (SPIs) in terms of proton conductivity, membrane swelling behavior, membrane stability toward water, and fuel cell performance in polymer electrolyte fuel cells (PEFCs) or direct methanol fuel cells (DMFCs). The structure-property relationship of SPI membranes is discussed in details with respect to the chemical structure of various sulfonated diamines and morphology of SPI membranes from the viewpoints of viscosity, mechanical strength and proton conductivity. Ion exchange capacity (IEC), basicity of sulfonated diamine, configuration (para-, meta-, or ortho-orientation) and chemical structure of polymer chain (linear or net-work) show great influence on the water stability and mechanical strength of SPI membrane. The SPIs with a branched/crosslinked structure and derived from highly basic sulfonated diamines display reasonably high water stability of more than 200–300 h in water at 130 °C, suggesting high potential as PEMs operating at temperatures up to 100 °C. The SPI membranes have fairly high proton conductivity at higher relative humidities and low methanol permeability. The water and methanol crossover through membrane under the fuel cell operation conditions is not controlled by electro-osmosis due to proton transport but by diffusion due to activity difference. This is quite different from the case of perfluorosulfonated membranes such as Nafion and results in the advantageous effects on fuel cell performance. SPI membranes displayed high PEFC performances comparable to those of Nafion 112. In addition, SPI membranes displayed higher performances in DMFC systems with higher methanol concentration (20–50 wt %), which is superior to Nafion and have high potential for DMFC applications at mediate temperatures (40–80 °C). [DOI 10.1295/polymj.38.197]

KEY WORDS Branching / Crosslinking / Fuel Cell Performance / Sulfonated Diamine / Sulfonated Polyimide / Polymer Electrolyte Membrane / Proton Conductivity / Water Stability / Hydrolysis Stability /

In the past decades, great interest has been focused on the development of polymer electrolyte fuel cells (PEFCs) and direct methanol fuel cells (DMFCs) as a clean power source of energy for transportation, stationary and portable power applications.[1,2] Fuel cells with high performance, high durability and potentially lower cost are greatly required. Polymer electrolyte membrane (PEM) is one of the key components in PEFC and DMFC systems. Perfluorosulfonic acid copolymer membranes, such as DuPont's Nafion membrane, are the state-of-the-art PEMs commercially available due to their high proton conductivity and excellent chemical stability.[3,4] However, because of their high cost, low operational temperature below 80 °C and large methanol crossover, there has been much interest in alternative PEMs. Many efforts have been done in the development of PEMs based on sulfonated aromatic hydrocarbon polymers.[5–9] The main problem existed in the hydrocarbon PEMs is the membrane stability under fuel cell conditions and low conducting performance at low moisture atmosphere. The balance between ion exchange capacity (IEC), proton conductivity and mechanical stability of a PEM plays an important role on its comprehensive performance in a fuel cell.

It is well known that aromatic polyimides have found wide applications in many industrial fields due to their excellent thermal stability, high mechanical strength, good film forming ability, and superior chemical resistance. These merits are just what are required for the polyelectrolyte membrane materials employed in fuel cell systems. Sulfonated naphthalenic polyimides (SPIs) with six-membered imide rings have been developed as promising candidates for PEFCs. Mercier and his coworkers developed sulfonated block copolyimides (co-SPIs) from 1,4,5,8-naphthalenetetracrboxylic dianhydride (NTDA), 2,2′-benzidinedisulfonic acid (BDSA, a commercially available sulfonated diamine) and common nonsulfonated diamines.[10–14] The sulfonated block copoly-

†To whom correspondence should be addressed (Tel: +81-836-85-9660; Fax: +81-836-85-9601; E-mail: okamotok@yamaguchi-u.ac.jp).

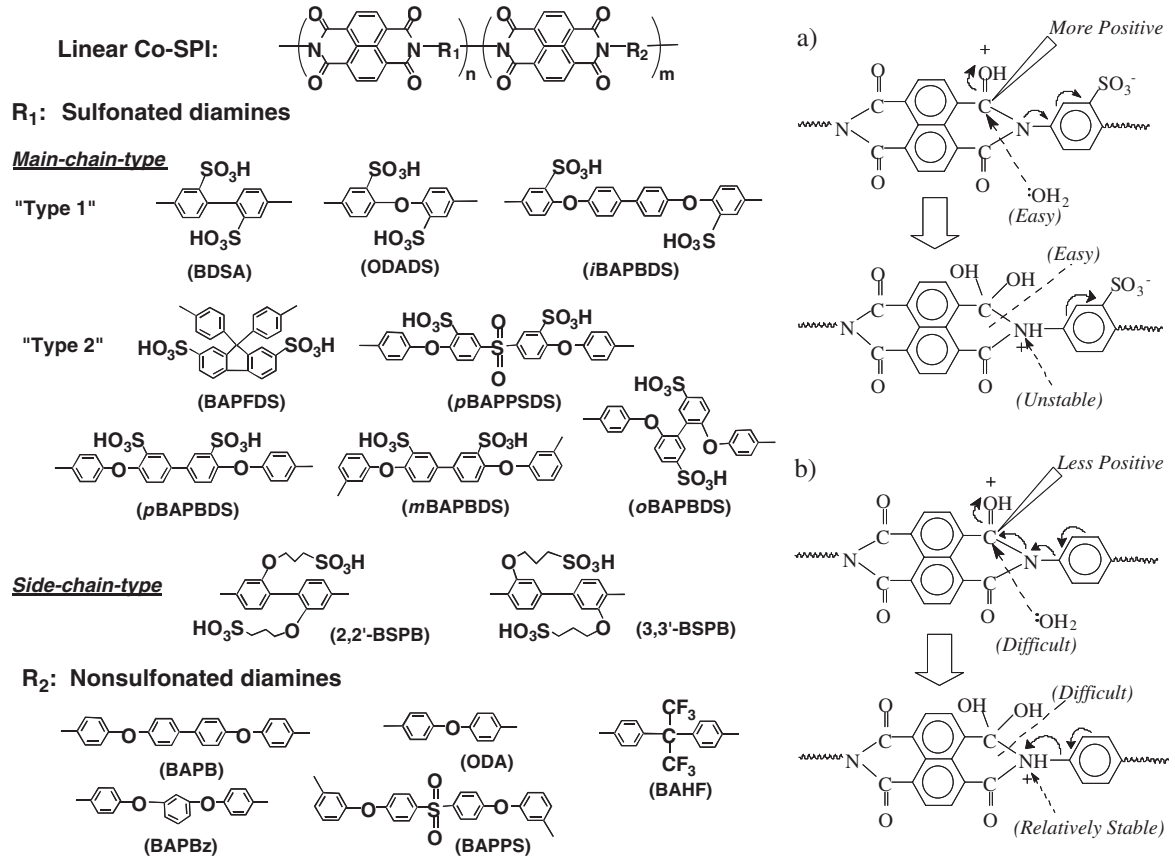


**Figure 1.** Chemical structure of NTDA-based SPIs.

imide membranes have been reported to show reasonably high performance in a $H_2/O_2$ fuel cell system at 60 °C for more than 3000 h. However, the proton conductivities of these membranes were rather lower due to their lower ion exchange capacity (IEC) values, which were essential for maintaining membrane durability toward water. This seems to limit the further improvement in PEFC performance.[14]

Other research groups have also reported the synthesis and proton conductivity of BDSA-based copolyimides with different nonsulfonated diamine moieties. Miyatake *et al.* have reported on high proton conductivities more than 0.2 S/cm at 100% relative humidity (RH) and high temperatures above 100 °C for their BDSA-based SPI membranes, whereas they did not mention the water stability.[15–18] Lee *et al.* have reported on the water stability up to 110 h at 80 °C for their BDSA-based SPI membranes.[19,20] Recently, the research group of Mercier and Diat *et al.* has reported on the aging of the BDSA-based block copolyimide membranes in PEFCs and in hot water.[21,22] The predominant aging mechanism was imide group hydrolysis, which was significantly accelerated above 80 °C. These results lead us to the view that a series of copolyimide membranes derived from NTDA, BDSA and different nonsulfonated diamines generally have poor water stability at temperatures above 80 °C.

This review presents an overview of the synthesis, membrane stability, chemical and electrochemical properties, and fuel cell applications of new proton-conducting polymer electrolyte membranes based on sulfonated polyimides that have been made during the past decade.

## WATER STABILITY OF SPI MEMBRANES DEVELOPED SO FAR (I)

Proton conductivity and membrane stability are two important factors that greatly affect the performance of a fuel cell system. High proton conductivity of a membrane requires large sulfonation degree or IEC. However, higher IEC generally leads to larger swelling degree or even dissolution in water of the membranes. Improving membrane stability and enhancing proton conductivity seems to be contradictory to each other. Therefore, IEC should be controlled at an appropriate level to balance the stability and conductivity as well as possible. Besides IEC, the chemical structure of polymers is another key factor affecting membrane stability and proton conductivity.

We synthesized novel sulfonated (co)polyimides from NTDA, novel different sulfonated diamines

**Table I.** IEC, WU and water stability of NTDA-based SPIs

| NTDA-based SPIs | IEC[a] (mequiv/g) | WU[b] (wt %) | Water stability | | Ref. |
|---|---|---|---|---|---|
| | | | T (°C) | Time (h) | |
| BDSA/ODA (1/1) | 1.98 | 79 | 80 | 5 | 24 |
| BDSA/BAPBz (1/1) | 1.82 | 77[c] 68[d] | 80 | 60 | 41 |
| BDSA/DDS (1/1) | 1.66 | 21 | 80 | 110 | 19 |
| ODADS/ODA (1/1) | 1.95 | 87 | 80 | 25 | 23 |
| ODADS/BAPB (1/1) | 1.68 | 57 | 80 | 200 | 23 |
| BAPFDS/ODA (2/1) | 2.09 | 76 | 80 | 20 | 24 |
| *o*BAPBDS/BAPB (2/1) | 1.89 | 152 | 80 | 105 | 27 |
| *i*BAPBDS/BAPB (2/1) | 1.89 | 62[e] | 100 | 200 | 29 |
| *m*BAPBDS/BAPB (3/2) | 1.73 | 47 | 100 | 500 | 29 |
| *p*BAPBDS/BAPB (2/1) | 1.89 | 63 | 100 | >1000 | 26 |
| *p*BAPBDS/BAPBz (2/1) | 1.96 | 70[c] 58[e] | 100 | >500 | 41 |
| *p*BAPPSDS/BAPPS (2/1) | 1.73 | 98[c] | 100 | >200 | 28 |
| *m*BAPPSDS/BAPPS (3/2) | 1.59 | 53[d] | 80 | 42 | 31 |
| DAPPS | 2.09 | 105[d] | 80 | 200 | 32 |
| 2,2′-BSPB | 2.89 | 220[d] | 100 | 2500 | 33 |
| 3,3′-BSPB | 2.89 | 250[d] | 100 | 700 | 33 |
| 2,2′-BSPB/BAPB (2/1) | 2.02 | 61[e] | 100 | >3000 | 34 |
| 3,3′-BSPB/BAPB (2/1) | 2.02 | 64[e] | 100 | >3000 | 34 |
| 2,2′-BSPOB/BAPB (2/1) | 1.88 | 78[e] | 100 | >3000 | 37 |
| 3,3′-BSPOB/BAPB (2/1) | 1.88 | 55[e] | 100 | >3000 | 37 |
| DASSPB/BAPBz (2/1)-s | 1.64 | 47[e] | 100 | >300 | 38 |
| BAPSBPS/BAPBz (2/1) | 1.52 | 31[e] | 100 | >300 | 39 |
| *p*BAPBDS/TAPB (6/1) | 2.29 | 77[e] | 100 | >3000 | 40 |
| 3,3′-BSPB/TAPB (6/1) | 2.49 | 114[e] | 130 | >200 | 40 |

[a]Calculated value. [b]At 80 °C. [c]At 100 °C. [d]At 50 °C. [e]At 30 °C.

(SDAs) and non sulfonated diamines, of which the chemical structures are shown in Figure 1, and investigated the relationship between the chemical structure and water stability of the SPI membranes.[23–28] We classified the sulfonated diamines into two groups. The sulfonated diamines such as BDSA, 4,4′-diamino-diphenyl-ether-2,2′-disulfonic acid (ODADS) and 4,4′-bis(4-amino-2-sulfophenoxy)biphenyl (*i*BAPBDS), where the electron-withdrawing sulfonic acid groups are bonded directly to the amino-phenyl rings, are noted as "Type 1". On the other hand, "Type 2" diamines developed, where the sulfonic acid groups are bonded to aromatic rings other than the amino-phenyl rings, are 4,4′-bis(4-aminophenoxy)biphenyl-3,3′-disulfonic acid (*p*BAPBDS), 4,4′-bis(3-aminophenoxy)biphenyl-3,3′-disulfonic acid (*m*BAPBDS), 2,2′-bis(4-aminophenoxy)-biphenyl-5,5′-disulfonic acid (*o*BAPBDS), 9,9-bis(4-aminophenyl)-fluorene-2,7-disulfonic acid (BAPFDS), and bis[4-(4-aminophenoxy)-phenyl]sulfone-3,3′-disulfonic acid (*p*BAPPSDS). Among these SDAs mentioned above, the *p*-, *m*-, *o*-, *i*-BAPBDS are isomers to each other. The water stability was evaluated by the elapsed time until the membrane hydrated in water lost the mechanical property. The loss of mechanical property was judged when the membrane broke after being lightly bent in the case of the soaking at 80 °C or when the membrane began to break into pieces under boiling in the case of soaking at 100 °C.[26] The data are summarized in Table I.

The water stability was a result of the total effect of solubility stability, hydrolysis stability, and swelling-stress stability. The solubility stability was mainly determined by the IEC and the configuration of sulfonated diamine moiety. High IEC generally leads to large water uptake and thus high swelling degree or even dissolution of membrane in water, indicating poor water stability. The BDSA-based co-SPIs shown in Table I with IECs of 1.98, 1.82 and 1.66 meq $g^{-1}$ displayed water stability of 5, 60 and 110 h, respectively, at 80 °C. Except for the effect of nonsulfonated diamine, IEC may play a dominant role on their water durability. Beside IEC, the chemical structure also had large influence on water stability of the SPI membranes. As shown in Table I, for example, NTDA-ODADS/ODA (1/1) and NTDA-BDSA/ODA (1/1), had almost the same IEC but quite different water stability. The former could maintain mechanical strength after being soaked in water at 80 °C for 25 h, which was much longer than that of the latter, and we have ascribed such a difference in water stability to their different chain flexibility.[23] NTDA-ODADS/ODA

(1/1) has fairly flexible structure due to the flexible linkage of ether bond in ODADS moiety (and thus flexible main chain), whereas NTDA-BDSA/ODA (1/1) is rather rigid because the two phenyl rings of BDSA cannot freely rotate along the axis due to the steric effect of the two bulky sulfonic acid groups. Flexible chain can undergo easier relaxation of polymer chain against membrane swelling to reduce swelling stress than the rigid one, and this is likely the main reason for the better water stability of NTDA-ODADS/ODA (1/1). In addition, we have also postulated that the high basicity of SDAs is a favorable factor for improving water stability of the resulting SPIs.[24] It is well known that aromatic diamines with higher basicity are generally more reactive with dianhydrides than those with lower basicity. Since hydrolysis is the reverse reaction of polymerization, SPIs derived from highly basic diamines should give much better hydrolysis stability than those from weakly basic ones. As shown in Table I, by only using the effect of chain flexibility, it is difficult to explain the relatively good water stability of NTDA-BAPFDS/ODA (2/1) in comparison with that of NTDA-BDSA/ODA (1/1) because BAPFDS moiety is also highly rigid and bulky and its IEC is even slightly larger. An obvious difference in structure between BAPFDS and BDSA is that the former belongs to "Type 2" SDA and the latter belongs to "Type 1", as classified as mentioned above. Because of the strong electron-withdrawing effect resulting from the sulfonic acid groups, the electron density of the phenyl rings where the amino groups are bonded should be higher for BAPFDS than for BDSA, that is, the "Type 2" SDAs are more basic than the "Type 1" ones. The schematic diagram of hydrolysis for SPIs derived from "Type 1" and "Type 2" diamines is also shown in Figure 1. For "Type 1" SDA-based polyimides, the protonated nitrogen is less stable because the positive charge in nitrogen cannot be well dispersed due to the low electron density of the phenyl ring to which the amino group and the sulfonic acid group are bonded (Figure 1a), and therefore the cleavage of the carbon–nitrogen bond is fairly easy. On the contrary, for "Type 2" SDA-based polyimides, the nitrogen is relatively stable because the positive charge in nitrogen is well dispersed due to the electron donor effect of the phenyl ring to which the amino group is bonded, and thus the cleavage of the carbon–nitrogen bond is relatively difficult. As a result, "Type 2" SDA-based polyimides are difficult to hydrolyze in comparison with "Type 1" SDA-based ones (Figure 1b), which is just consistent with the experimental results of water stability measurement. Correspondingly, it is no surprise that NTDA-BAPFDS/ODA (2/1) displayed better water stability than NTDA-BDSA/ODA (1/1).

Besides IEC, flexibility and basicity of sulfonated diamine, configuration of SPIs also had great influence on the membrane stability toward water. As listed in Table I, the BAPBDS-based SPI membranes displayed significant difference in water stability. *p*-, *m*-, *o*- and *i*BAPBDS are isomeric sulfonated diamines belong to "Type 2" except for *i*BAPBDS belongs to "Type 1". It is reasonable to understand the much better water stability of the *p*- and *m*BAPBDS-based co-SPIs than *i*BAPBDS-based one, due to the high basicity of the former SDAs. However, it was found that the *o*BAPBDS-based co-SPI showed poorer water stability than the *i*BAPBDS-based one, although the former SDA was more basic. In fact, the difference in configuration for these isomeric diamines led to quite different solubility behavior of the resulting SPIs in common organic solvents and in water.[29] The para-oriented structure of the *p*BAPBDS- and *i*BAPBDS-based SPIs showed rather poor solubility in aprotic solvents such as DMSO and DMF. However, ortho-oriented (*o*BAPBDS) and the meta-oriented (*m*BAPBDS)-based SPIs displayed fairly good solubility properties. The homo-SPI of NTDA-*o*BAPBDS and NTDA-*m*BAPBDS were even soluble in water by heating. The introduction of hydrophobic nonsulfonated diamine led to decrease in solubility and thus improvement in water stability. Consequently, *o*BAPBDS-based co-SPI displayed the lowest water stability compared to other isomers-based ones, due to its better solubility property rather than hydrolysis. In short, the para-, meta-, and ortho-oriented structure had increased solubility behavior and thus decreased water stability in that order. As a result, as shown in Table I, the *p*BAPBDS-based SPIs with para-oriented configuration, moderate IEC, highly basic diamine moiety, and more flexible structure displayed much better water stability than the SPIs based on other sulfonated diamines. The similar effect of difference in configuration on water stability was also observed for BAPPSDS-based SPIs. For example, McGrath *et al.* have reported on novel co-SPIs based on bis[4-(3-aminophenoxy)phenyl]sulfone-3,3′-disulfonic acid (*m*BAPPSDS).[30,31] As listed in Table I, the *m*BAPPSDS-based co-SPIs displayed rather poor water stability. NTDA-*m*BAPPSDS/BAPPS (3/2) membrane became brittle after soaking in water for 42 h at 80 °C. While the *p*BAPPSDS-based co-SPI showed much better water stability and could endure soaking in water at 100 °C for more than 200 h.[28]

The above-mentioned SPIs are the main-chain-type ones, where the sulfonic acid groups are bonded directly to aromatic rings composing polymer main chains. We also synthesized side-chain-type SPIs bearing pendant sulfoalkoxy groups, such as 2,2′-bis(3-sulfopropoxy)benzidine (2,2′-BSPB) and 3,3′-bis(3-sulfo-

**Table II.** Physical properties of NTDA-based SPI membranes

| Code No. | SPIs | IEC[a] (meq/g) | $[\eta]$[b] (dL/g) | $WU$[c] (wt %) | Size change $\Delta t_c$ | Size change $\Delta l_c$ | $T_{d1}$ (°C) |
|---|---|---|---|---|---|---|---|
| M1 | *p*BAPBDS | 2.63 | 1.73 | 115[d] | 0.32 | 0.087 | — |
| M2-1 | *p*BAPBDS/BAPB (2/1) | 1.89 (1.86) | 1.03 | 80 | 0.37 | 0.063 | — |
| M2-2 | *p*BAPBDS/BAPB (2/1) | 1.89 (2.0) | 2.7 | 51 | 0.20 | 0.044 | — |
| M2-3 | *p*BAPBDS/BAPB (2/1) | 1.89 | 4.4 | 57 | 0.14 | 0.049 | — |
| M3-1 | *p*BAPBDS/BAPBz (2/1) | 1.96 | (4.9) | 58 (70[e]) | 0.10 | 0.070 | 309 |
| M3-2 | *p*BAPBDS/BAPBz (2/1) | 1.96 | (7.7) | 53 | 0.14 | 0.065 | — |
| M3-3 | *p*BAPBDS/BAPBz (2/1) | 1.96 | (2.0) | 55 | 0.14 | 0.070 | — |
| M4 | *p*BAPBDS/BAPPS (3/2)-s | 1.66 | 1.83 | 48 | 0.15 | 0.047 | 309 |
| M5 | BDSA/BAPBz (1/1) | 1.82 | (3.3) | 68 (77[e]) | 0.20 | 0.03 | — |
| M6-1 | 2,2′-BSPB/BAPB (2/1) | 2.02 | — | 76[d] | 0.49 | 0.047 | 232 |
| M6-2 | 2,2′-BSPB/BAPB (2/1) | 2.02 | 4.5 | 72 | 0.47 | 0.043 | 248 |
| M7 | 2,2′-BSPB/BAPB (2/1)-s | 2.02 | — | 87 | 0.55 | 0.045 | 255 |
| M8 | 2,2′-BSPB/BAPPS (2/1) | 1.95 | — | 39[d] | 0.10 | 0.023 | 254 |
| M9-1 | 3,3′-BSPB/BAPB (2/1) | 2.02 (1.72) | — | 62[d] | 0.48 | 0.030 | — |
| M9-2 | 3,3′-BSPB/BAPB (2/1) | 2.02 (1.73) | 5.7 | 64 | 0.39 | 0.034 | 252 |
| M10 | 2,2′-BSPOB/BAPB (2/1) | 1.88 | 3.9 | 78 | 0.39 | 0.026 | 300 |
| M11 | 2,2′-BSPOB/BAPBz (1/1)-s | 1.56 | 2.9 | 57 | 0.24 | 0.024 | — |
| M12 | 3,3′-BSPOB/BAPB (2/1) | 1.88 | 2.1 | 55 | 0.24 | 0.034 | 310 |
| M13 | DASSPB/BAPBz (2/1)-s | 1.64 | 1.0 | 47 | 0.10 | 0.090 | 310 |
| M14 | DASSPB/BAHF (2/1)-s | 1.99 | — | 60 | 0.13 | 0.12 | — |
| M15 | BAPSBPS/BAPBz (2/1) | 1.52 | 0.8 | 31 | 0.23 | 0.040 | 350 |
| M16 | *p*BAPBDS/TAPB (6/1) | 2.29 (2.32) | — | 77 | 0.23 | 0.077 | — |
| M17 | *p*BAPBDS/TAPB (6/1) (chemical imidization) | 2.29 | — | 62 | 0.27 | 0.032 | — |
| M18 | 2,2′-BSPB/TAPB (7.5/1) | 2.57 | — | 104 | 0.59 | 0.012 | 256 |
| M19 | 3,3′-BSPB/TAPB (6/1) | 2.49 | — | 114 | 0.68 | 0.020 | — |

[a]Calculated values, the data in parenthesis are measured values by titration. [b]Intrinsic viscosity at 35 °C, the data in parenthesis are reduced viscosity measured at 0.5 g/dL in *m*-Cresol. [c]At 30 °C. [d]At 50 °C. [e]At 100 °C.

propoxy)benzidine (3,3′-BSPB), of which the chemical structures are also shown in Figure 1, and investigated the water stability of their membranes.[32–34] The data are also summarized in Table I. The side-chain-type SPIs based on 2,2′-BSPB and 3,3′-BSPB displayed much better water stability than the main-chain-type SPIs. This may partly come from the higher basicity of the diamine moieties due to the electron-donating effect of alkoxy groups. Furthermore, the microphase-separated structure also plays an important role on their high water stability. Note that the flexible sulfopropoxy groups are favorable to aggregate into hydrophilic domains and the polyimide backbones form hydrophobic domains. As a result, a microphase separation structure composed of hydrophilic domains and hydrophobic moieties was well formed.[34] Because the hydrolysis of imide ring is an acid-catalytic reaction, if the protons are mostly restricted in the ion-rich domains isolated from the polymer main chain, the hydrolysis of imide ring of the SPI will be depressed. This is likely another reason for the excellent water stability of NTDA-BSPB. Asano *et al.* also reported on the excellent hydrolytic stability of 3,3′-BSPB-based co-SPIs.[35]

## WATER STABILITY OF LINEAR AND BRANCHED/CROSSLINKED SPI MEMBRANES (II)

Based on the results developed so far, *p*BAPBDS-based SPIs and side-chain-type SPIs tend to have better water stability at high temperature and fully hydrated state. Table II shows the physical properties of a series of SPIs from *p*BAPBDS and 2,2′- or 3,3′-BSPB. The SPIs with same chemical composition displayed different viscosities and correspondingly different properties in many fields, which will be discussed in the next part. Novel side-chain-type SPIs bearing aromatic sulfonated side chains were synthesized from 3,3′-bis(4-sulfophenoxy)benzidine (3,3′-BSPOB),[36,37] 2,2′-bis(4-sulfophenoxy)benzidine (2,2′-BSPOB),[37] 3,5-diamino-3′-sulfo-4′-(4-sulfophenoxy) benzophenone (DASSPB)[38] and 4,4′-bis(4-aminophenyl)-2,2′-bis[4-(4-sulfophenyl)-2-sulfobenzoyl]-1,1′-diphenyl sulfone (BAPSBPS),[39] of which the chemical structures are shown in Figure 2. To further improve the mechanical stability of SPI membranes, branched/crosslinked SPIs (B/C-SPIs) derived from *p*BAPBDS,

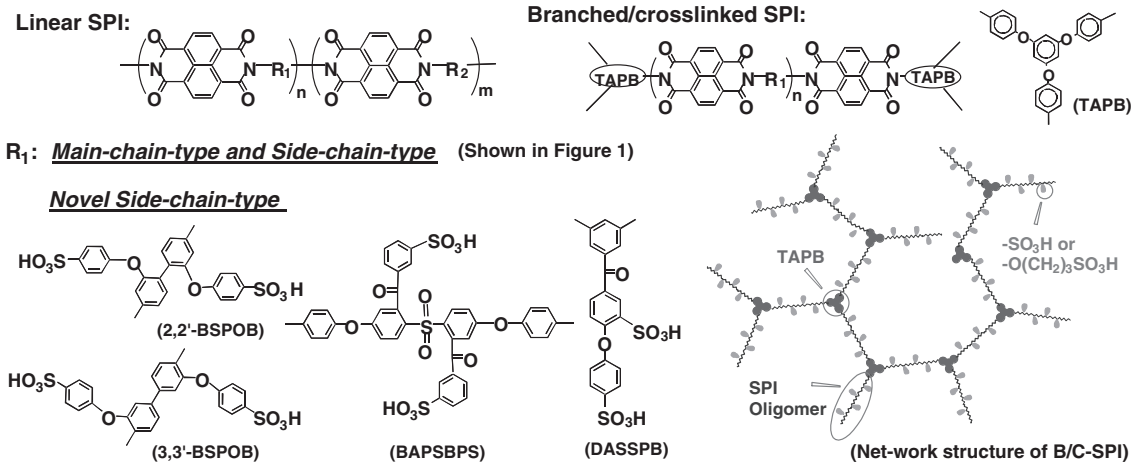


**Figure 2.** Chemical structure of novel side-chain-type linear SPIs and schematic diagram of B/C-SPIs.

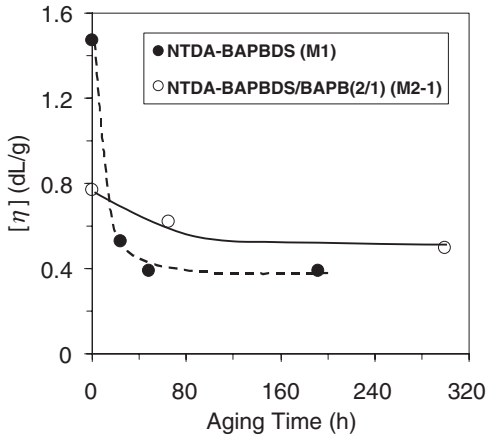


**Figure 3.** Variation in [$\eta$] of SPIs with aging in water at 100 °C.

2,2′-BSPB and 3,3′-BSPB were developed by using 1,3,5-tris(4-aminophenoxy)benzene (TAPB), a triamine with flexible ether linkages, as a branching/crosslinking agent.[40] The chemical structure of B/C-SPIs is presented in Figure 2. The B/C-SPI membranes had a net-work structure and were not soluble in any solvents, and as a result displayed much better water stability than the corresponding linear SPI membranes, as listed in Table I. The physical properties of these newly-developed SPIs are also listed in Table II. In this section, the membrane stability toward aging in water at 100 or 130 °C is investigated in details with respect to changes in viscosity, mechanical properties, weight loss, proton conductivity and spectral analysis.[41]

*Intrinsic Viscosity*

Figure 3 shows variation in intrinsic viscosity [$\eta$] with soaking time in water at 100 °C for *p*BAPBDS-based homo-SPI and co-SPI with relatively low viscosity. It should be noted that the SPI samples soaked in water were all in proton form. Since the SPIs in proton form were not soluble in any solvents but those in TEA salt form dissolved in *m*-cresol. So, in the measurement of viscosity, the SPI samples in proton form were changed into their TEA salt form using 0.1 wt % TEA solution. However, with the ion-exchange procedure, the base-catalyzed hydrolysis of polymer chain took place to a certain extent, resulting in a decrease in [$\eta$]. For example, the reduction in [$\eta$] with the ion-exchanging procedure for *p*BAPBDS-based homo-SPI and co-SPI was 15 and 25% from their original values of 1.73 and 1.03 dL/g down to 1.47 and 0.77 dL/g, respectively. So, in evaluation of the data in Figure 3, we should take into account that the actual [$\eta$] values of the soaked membranes might be somewhat larger than the observed values. As shown in Figure 3, for NTDA-*p*BAPBDS, the [$\eta$] decreased down to a third of the original value after the soaking at 100 °C for 24 h, but did not further decrease after 50 h. The initial decrease in [$\eta$] was smaller for NTDA-*p*BAPBDS/BAPB (2/1), although its initial [$\eta$] was as low as 0.8 dL/g, and it kept a high [$\eta$] value of 0.5 dL/g even after 300 h. This indicates that the polymer chain scission caused by the hydrolysis of imide ring occurred in the initial period of the soaking but very slowly in the further soaking and the molecular weight might be kept at a reasonable level for further prolonged soaking at 100 °C. This may be the reason that the *p*BAPBDS-based SPI membranes kept their sheet-shape in boiling water for more than 1000 h as mentioned in Table I. These results suggest the presence of some parts being less stable against the hydrolytic scission in polymer chains than other parts. Hydrolytic polymer chain scission seems to take place fast there in the early stage and then slowly in other parts.

According to the paper by McGrath *et al.*, NTDA-*m*BAPPSDS/BAPPS (3/2) membrane became brittle

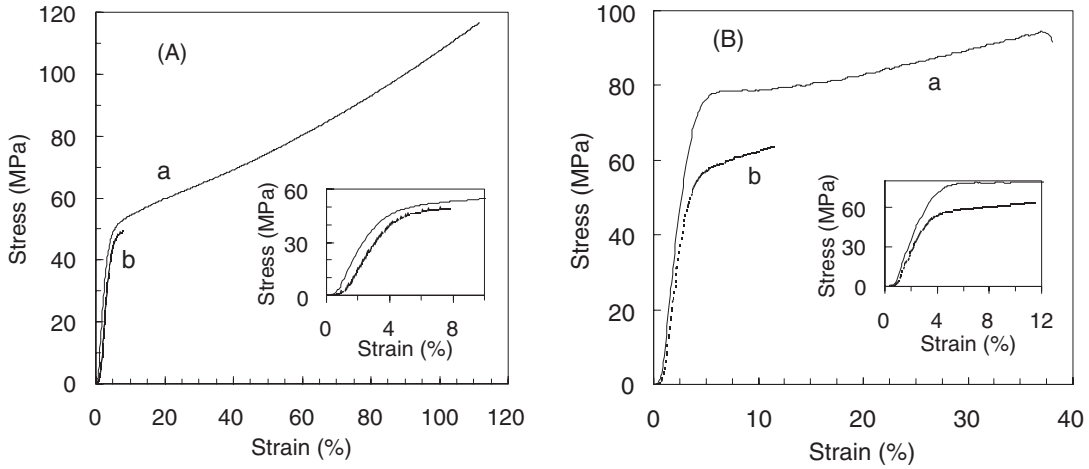


**Figure 4.** Stress-strain curves of SPI membranes (a) before and (b) after aging in water. (A) **M2-3**, aged at 100 °C for 300 h, (B) **M11**, aged at 130 °C for 300 h.

after soaking in water for 42 h at 80 °C followed by the significant decrease in intrinsic viscosity from an original value of 2.51 dL/g down to 0.38 dL/g.[31] As a result, the *p*BAPBDS-based SPIs, the para-isomer in the present study, displayed much better water stability and smaller reduction in $[\eta]$. It seems reasonable to consider that the para-isomers give better water stability than the meta-isomers, as discussed in the former part.

*Mechanical Properties*

Mechanical property stability of SPI membrane is an important factor affecting membrane performance with respect to lifetime. The mechanical properties were evaluated by means of tensile strength and membrane toughness. The membrane toughness level was specified as follows. In level I, the membrane is brittle and breaks into pieces by handling. In level II, the membrane sheet breaks when being bent by holding both ends between fingers. In level III, the membrane sheet breaks along a fold when it is folded to zero degree. In level IV, the membrane sheet breaks when it is folded back. In level V, the membrane sheet does not break after it is folded back. The typical stress-strain curves of SPI membranes before and after aging in water at 100 °C are shown in Figure 4A. The un-aged sample displayed a large elongation after a yield point till a break point, whereas the aged sample displayed a much smaller elongation. As a result, the aged sample showed smaller maximum stress and much smaller elongation degree at break point compared to the un-aged one, although the Young's modulus was not so different between them. As can be seen from Table III, such a change in the tensile strength property took place mainly in the initial period (48–96 h) of the soaking and the further soaking till 300 h slightly reduced the tensile strength property. This behavior is similar to the viscosity change with the soaking time mentioned above. So, after soaking for 300 h, the *p*BAPBDS-, 2,2′-BSPB- and 3,3′-BSPB-based SPI membranes still kept reasonably high Young's modulus and maximum stress more than 1 GPa and 40 MPa, respectively, and also fairly high membrane toughness level of V or IV.

As shown in Table IV, in the case of aging in water at 130 °C, the similar change in the tensile strength property took place within 24 h, and the further soaking very slightly reduced the tensile strength property. Comparison among the *p*BAPBDS-based co-SPIs (**M2**–**M4**) shows that the tensile strength property was similar before the aging but slightly different after the aging. This might be due to some effect of nonsulfonated diamine structure and/or polymer segment structure as well as small difference in membrane morphology between different preparation batches. After soaking for 96 or 192 h, these *p*BAPBDS-based SPI membranes still kept reasonably high Young's modulus and maximum stress more than 0.6 GPa and 30 MPa, respectively, and also high membrane toughness level of V. Furthermore, the 2,2′- or 3,3′-BSPOB-based side-chain-type co-SPI membranes (**M10**–**M12**) had high Young's modula above 2.0 GPa and maximum stress values of 60–70 MPa, after aging for 192 or 300 h, which were larger than those of the BAPBDS-based ones. Especially, judging from the appearance of membrane just after the soaking and high mechanical strength shown in Figure 4B, **M11** is considered to have the water stability of 500 h or more in water at 130 °C. On the other hand, the BDSA-based co-SPI membrane (**M5**) is noted to completely loose its mechanical strength after soaking for 24 h, indicating much poorer hydrolytic stability than the *p*BAPBDS- and 2,2′- or 3,3′-BSPOB-based SPIs. The change in the mechanical properties with the

**Table III.** Properties of NTDA-based SPI membranes before and after aging in water at 100 °C

| Code No. | Soaking Time (h) | Weight loss (%) | S loss (mol %) | σ (50 °C, mS/cm) | | | | *YM* (GPa) | *MS* (MPa) | *EB* (%) | Toughness |
|---|---|---|---|---|---|---|---|---|---|---|---|
| | | | | In water | 90% | 70% | 50% RH | | | | |
| M2-1 | 0 | | | 140 | 89 | 28 | 2.5 | 1.6 | 85 | 80 | V |
| | 96 | 0.5 | 1.7 | — | — | — | — | 1.4 | 37 | 8 | V |
| | 192 | — | 1.7 | 131 | 91 | 28 | 2.8 | — | — | — | V |
| | 300 | 2.0 | 2.9 | — | — | — | — | 1.6 | 40 | 4 | IV |
| M2-3 | 0 | | | — | — | — | — | 1.8 | 120 | 120 | V |
| | 300 | 2.8 | 1.7 | — | — | — | — | 1.6 | 49 | 8 | V |
| M3-2 | 0 | | | — | — | — | — | 1.6 | 81 | 90 | V |
| | 96 | 0.1 | 1.3 | — | — | — | — | 1.4 | 45 | 6 | V |
| | 300 | 5.2 | 3.2 | — | — | — | — | 1.4 | 47 | 6 | V |
| M6-1 | 0 | | | 138 | 99 | 9.1 | 1.0 | — | — | — | V |
| | 48 | — | 22 | 96 | 80 | 4.4 | 0.07 | — | — | — | V |
| | 300 | — | 21 | 113 | 93 | 1.4 | 0.05 | — | — | — | IV |
| M6-2 | 0 | | | 154[a] | 95[a] | 15.4[a] | 2.8[a] | 2.1 | 127 | 86 | V |
| | 48 | 2.2 | 11 | 130[a] | 75[a] | 7.8[a] | 1.2[a] | 2.3 | 68 | 12 | V |
| | 200 | 9.6 | 17 | 146[a] | 80[a] | 9.6[a] | 1.5[a] | 1.7 | 57 | 6 | IV |
| M7 | 0 | | | 113 | 101 | 8.0 | 0.85 | — | — | — | V |
| | 48 | — | 3.0 | 98 | 90 | 16 | 1.6 | — | — | — | V |
| | 300 | — | 5.0 | 93 | 90 | 11 | — | — | — | — | V |
| M8 | 0 | | | 47 | 18 | 3.9 | 0.04 | — | — | — | V |
| | 48 | — | 4.0 | 54 | 24 | 3.5 | 0.03 | — | — | — | V |
| | 300 | — | 6.0 | 46 | 29 | 2.6 | 0.05 | — | — | — | V |
| M9-1 | 0 | | | 121[a] | 116[a] | 23[a] | 2.3[a] | — | — | — | V |
| | 48 | — | 13 | 104[a] | 114[a] | 19[a] | 1.7[a] | — | — | — | V |
| | 300 | — | 11 | 118[a] | 109[a] | 9.1[a] | 1.2[a] | — | — | — | IV |
| M9-2 | 0 | | | 135[a] | 107[a] | 16[a] | 1.6[a] | 1.9 | 172 | 84 | V |
| | 48 | 4.1 | 22 | 99[a] | 49[a] | 6.9[a] | 0.64[a] | 1.9 | 113 | 41 | V |
| | 300 | 6.1 | 22 | 99[a] | 53[a] | 7.0[a] | 0.61[a] | — | — | — | IV |

[a]Measured at 60 °C.

aging in 100% RH vapor at 130 °C was similar to that with the aging in water at the same temperature.

The *p*BAPBDS- or BSPB-based B/C-SPI membranes showed much better water stability from the viewpoint of mechanical property than the corresponding linear SPI membranes. After aging in water at 130 °C for 192 h, NTDA-*p*BAPBDS/TAPB (6/1) (**M16**, **M17**) showed Young's modulus, maximum stress and elongation degree at break point of 0.9 GPa, 50 MPa and 14%, respectively. The corresponding values for NTDA-3,3′-BSPB/TAPB (6/1) (**M19**) were 2.0 GPa, 90 MPa and 12%. The network structure was effective to keep the mechanical strength at high level as possible as for long soaking time.

As mentioned above, the commonly observed behavior with the aging in water at high temperatures was a significant decrease in large elongation after a yield point till a break point and the corresponding reduction in maximum stress, which was due to the reduced effect of polymer chain entanglement as a result of polymer chain scission. This took place mainly in the early period of the aging and further reduction in the tensile strength properties with the prolonged aging was rather small and most of the SPI membranes especially for the B/C-SPI ones kept their mechanical properties at a reasonably high level.

*Weight Loss and Spectroscopic Analysis*

The data of weight loss and sulfur loss against the aging experiment are listed in Tables III and IV. With some exceptions, both weight loss and sulfur loss increased with an increase in aging time and also with an increase in aging temperature. In the case of some *p*BAPBDS-based SPI membranes (**M2**–**M4**, **M16**, **M17**), the weight loss and S loss with aging in water at 100 °C for 300 h were as small as 2–5 wt % and 2–3 mol %, respectively, whereas they became as large as 7–10 wt % and 4–9 mol %, respectively, at 130 °C for 96–192 h. The latter values were not so small. On the other hand, the BDSA-based co-SPI membrane displayed extremely large weight loss and S loss of 37 wt % and 46 mol %, respectively, at 130 °C for only 24 h, and broke into pieces.

In the case of 2,2′-(or 3,3′)-BSPB-based SPI membranes (**M6**–**M9**, **M18**, **M19**), both weight loss and S loss were larger compared with the *p*BAPBDS-based

**Table IV.** Properties of NTDA-based SPI membranes before and after aging in water at 130 °C

| Code No. | Soaking Time (h) | Weight loss (%) | S loss (mol %) | σ (50 °C, mS/cm) | | | | *YM* (GPa) | *MS* (MPa) | *EB* (%) | Toughness |
|---|---|---|---|---|---|---|---|---|---|---|---|
| | | | | In water | 90% | 70% | 50% RH | | | | |
| M2-2 | 0 | | | 117 | 94 | 18 | 2.3 | 1.2 | 100 | 120 | V |
| | 24 | 8.3 | 1.8 | 94 | 86 | 16 | 2.0 | 0.80 | 44 | 6 | V |
| | 48 | 7.6 | 4.0 | 91 | 86 | 16 | 2.1 | 0.81 | 40 | 6 | V |
| | 96 | 7.0 | 6.5 | — | — | — | — | 0.61 | 34 | 6 | V |
| M3-2 | 0 | | | — | — | — | — | 1.3 | 64 | 95 | V |
| | 24 | 3.6 | 7.5 | — | — | — | — | 1.3 | 33 | 6 | V |
| | 96 | 10 | 12 | — | — | — | — | 1.1 | 30 | 6 | V |
| M3-3 | 0 | | | 102[a] | — | 13[a] | 2.3[a] | 1.4 | 81 | 95 | V |
| | 192 | 7.3 | 8.1 | 103[a] | — | 13[a] | 2.9[a] | 1.2 | 55 | 10 | V |
| M4 | 0 | | | 91[a] | 77[a] | 19[a] | 3.2[a] | 1.2 | 78 | 94 | V |
| | 48 | 0.3 | 1.0 | 91[a] | 75[a] | 20[a] | 4.0[a] | 1.2 | 67 | 11 | V |
| | 48–96 | 7.0 | 2.6 | 87[a] | 72[a] | 16[a] | 3.5[a] | 1.1 | 62 | 12 | V |
| M5 | 0 | | | — | — | — | — | 2.6 | 85 | 50 | V |
| | 24 | 37 | 46 | Not measurable | | | | Not measurable | | | I |
| M10 | 0 | | | 168[a] | 128[a] | 30[a] | 7.0[a] | 2.9 | 122 | 45 | V |
| | 192 | 10 | 8.0 | 167[a] | 128[a] | 28[a] | 5.9[a] | 2.4 | 69 | 9 | V |
| M11 | 0 | | | 118[a] | — | 14[a] | 2.2[a] | 2.3 | 94 | 37 | V |
| | 300 | 8.6 | 13 | 120[a] | — | 10[a] | 3.0[a] | 2.2 | 64 | 11 | V |
| M12 | 0 | | | 143[a] | 104[a] | 17[a] | 2.0[a] | 2.5 | 111 | 35 | V |
| | 192 | 12 | 10 | 142[a] | 92[a] | 22[a] | 2.6[a] | 2.1 | 60 | 8 | V |
| M16 | 0 | | | 148 | 84 | 16 | 2.7 | 1.2 | 98 | 110 | V |
| | 48 | 6.6 | 5.7 | 142 | 98 | 17 | 2.4 | 0.90 | 55 | 10 | V |
| | 96 | 8.3 | 7.9 | 136 | 94 | 22 | 3.2 | 0.88 | 54 | 13 | V |
| M17 | 0 | | | 122 | 83 | 17 | 3.5 | 0.97 | 97 | 130 | V |
| | 48 | 3.7 | 4.8 | 120 | 83 | 17 | 3.9 | 0.91 | 50 | 13 | V |
| | 96 | 8.2 | 6.2 | 113 | 82 | 19 | 3.8 | 0.89 | 49 | 15 | V |
| | 192 | 9.4 | 7.2 | 114 | 89 | 18 | 4.0 | 0.91 | 48 | 14 | V |
| M18 | 0 | | | 150 | 95 | 12 | 1.7 | — | — | — | V |
| | 48 | 15 | — | — | 90 | 4.4 | 0.14 | 2.4 | 120 | 9 | V |
| | 96 | 13 | — | — | 67 | 1.7 | — | 2.3 | 83 | 5 | V |
| M19 | 0 | | | 147 | 128 | 11 | 1.1 | 2.3 | 120 | 18 | V |
| | 48 | 11 | 22 | 100 | 125 | 6.1 | 0.44 | 2.0 | 120 | 16 | V |
| | 96 | 10 | 22 | 91 | 109 | 6.1 | 0.34 | 1.93 | 110 | 17 | V |
| | 196 | 18 | 30 | 118 | — | 3.6 | 0.10 | 2.0 | 90 | 12 | V |

[a]At 60 °C.

SPIs. With the aging at 100 °C, the S loss significantly varied from membrane to membrane, that is, it was much smaller for NTDA-2,2′-BSPB/BAPB (2/1)-s (**M7**) and NTDA-2,2′-BSPB/BAPPS (2/1) (**M8**) than for NTDA-2,2′-BSPB/BAPB (2/1) (**M6**) and NTDA-3,3′-BSPB/BAPB (2/1) (**M9**). Pairs of 2,2′-(or 3,3′)-BSPB-based co-SPI, of which the chemical structure is the same and only the preparation batch was different, displayed significantly different S loss values.

The aging in 100% RH vapor at 130 °C gave much smaller weight and S losses than the aging in water for the *p*BAPBDS-based SPI membranes. For the BSPB-based SPI membranes, the similar behavior was also observed.

Figure 5 shows anion chromatograph spectra of soaking water solutions after aging SPI membranes in water at 130 °C for 48 h. The elution peaks around 13 min were attributed to $SO_4^{2-}$ ion produced by hydrolysis of sulfonic acid group. The hydrolysis decomposition degrees of sulfonic acid were 0.36 and 0.49 mol % at 130 °C for 24 and 96 h, respectively, for NTDA-*p*BAPBDS/BAPB (2/1), and 0.55 and 0.65 mol % at 130 °C for 48 and 196 h, respectively, for NTDA-3,3′-BSPB/TAPB (6/1). The small decomposition degree and its small increase with an increase in soaking time indicate the reasonably high hydrolysis stability of sulfonic acid for the *p*BAPBDS- and BSPB-based SPIs. In the case of the latter, a large peak appeared at an elution time of 3 min. The ion-chromatograph/MS analysis showed the $m/z$ value of this peak was 139, which was in agreement with that of $[HO(CH_2)_3SO_3]^-$. The cleavage of ether bond

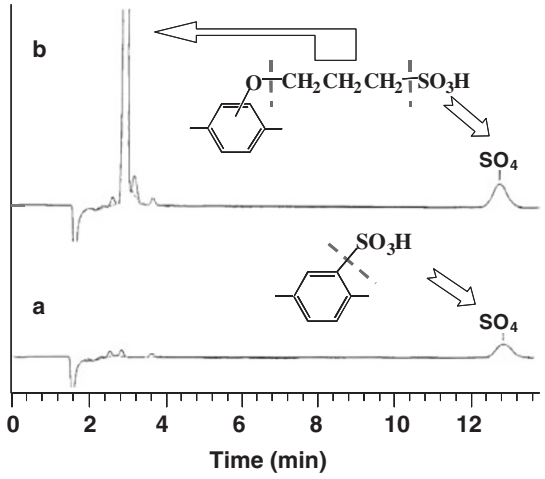


**Figure 5.** Anion chromatograph spectra of soaking water solutions after aging (a) **M2-2** and (b) **M19** in water at 130 °C for 48 h.

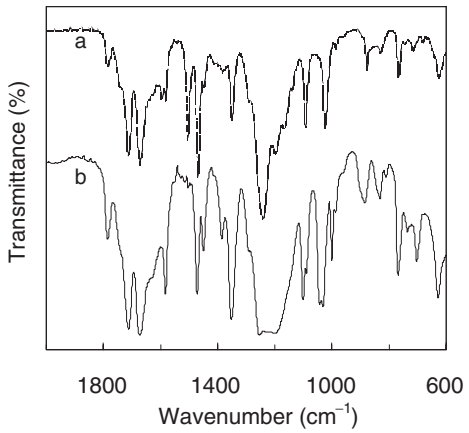


**Figure 6.** FT-IR spectra of the residue on distillation of soaking water solutions for (a) **M3-3** and (b) **M5** in KBr.

of sulfopropoxy group took place fairly easily at 130 °C for the BSPB-based SPIs.

The FT-IR spectra and $^1$H NMR spectra were measured for the residue on distillation of soaking water solutions for *p*BAPBDS- and BDSA-based co-SPIs (**M3-3** and **M5**) in Table IV. The FT-IR spectra are shown in Figure 6. They showed imide carbonyl (1712, 1668 cm$^{-1}$), acid carbonyl (1784 cm$^{-1}$), naphthalenic C=C (1581 cm$^{-1}$), imide C–N (1348 cm$^{-1}$) and O=S=O of sulfonic acid (around 1020 cm$^{-1}$). The $^1$H NMR spectra are shown in Figure 7. On the hydrolysis study of a naphthalenic imide model compound, Mercier *et al.* reported that the hydrolysis product of the imide–acid structure showed two doublets at 8.22 and 8.57 ppm.[42] They also demonstrated that the naphthalenic protons of copolyimide from NTDA, BDSA and 1,4-bis(4-aminophenoxy)-2-tertiobutyl-benzene showed a doublet peak at 8.74–8.78 ppm.[13] The naphthalenic protons of NTDA-based co-SPIs (in TEA salt form) dissolved in DMSO have

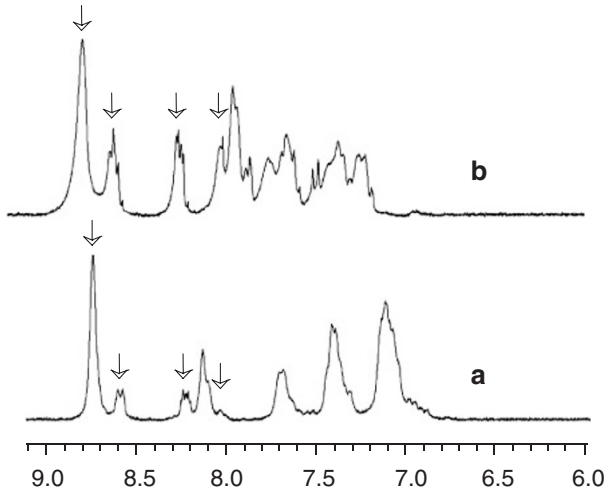


**Figure 7.** $^1$H NMR spectra of the residue on distillation of soaking water solutions for (a) **M3-3** and (b) **M5** in DMSO-$d_6$.

been reported to show a doublet-like peak at 8.7–8.8 ppm.[13,30] Therefore, the singlet peak at 8.75 and 8.80 ppm for NTDA-*p*BAPBDS/BAPBz (2/1) (**M3-3**) and NTDA-BDSA/BAPBz (1/1) (**M5**), respectively, in Figure 7 was attributed to equivalent naphthalenic protons of the imide–imide structure. The chemical shift was slightly larger for the latter SPI than for the former, because of the electron-withdrawing effect of sulfonic acid group on the amino-phenylene unit in BDSA moiety. The peaks at 8.58–8.64, 8.22–8.28 and 8.03 ppm in Figure 7 were attributed to naphtalenic protons of imide–acid, imide–acid, and acid–acid structures, respectively. The naphthalenic component ratio was evaluated from the peak ratios. The structure ratio of imide–imide:imide–acid:acid–acid was 1.00:0.32:0.04 for M3-3 and 1.00:0.67:0.30 for M5. It is noted that the content of the imide–imide structure is larger than those of the other structures. The protons of 2-, 4- and 5-positions of the central phenylene ring of BAPBz appear at 6.3–6.5 ppm. However, there was no peak in the range of 6.0 to 6.9 ppm in Figure 7, indicating no presence of BAPBz component in the residue of the soaking water. Therefore, the other peaks in the range of 7.0 to 8.2 ppm in Figure 7 were attributed to phenylene protons of BAPBDS and BDSA components. The ratio of sulfonated diamine component per naphthalenic one dissolved out into the soaking water was evaluated as 0.86 and 1.05 for **M3-3** and **M5**, respectively.

The above-mentioned facts lead us to the following conclusions about the hydrolysis. (1) With the aging in water at 130 °C, the polymer chain scission took place *via* the hydrolysis mainly on the imide (and/or isoimide and amide acid, if present) bonds neighboring sulfonated diamine residues but hardly on the bonds neighboring nonsulfonated diamine residues. (2) The hydrolysis took place much more easily for

the BDSA-based SPIs than for the *p*BAPBDS- and BSPB-based SPIs. (3) The component dissolved out in the soaking water was composed mainly of oligomers of NTDA and sulfonated diamine. Judging from the low ratios of imide–acid and acid–acid structure, the presence of insoluble part in the concentrated water solution and appreciable viscosity of the concentrated DMSO solution, the oligomers are considered to have two or three repeat units of imide–imide structure and one or two imide–acid structure at the chain end(s). The weight loss and S loss were rather larger for the BSPB-based SPIs than the *p*BAPBDS-based SPIs, because the sulfopropoxy groups, another hydrolysis product, easily dissolved out into water by the soaking.

*Proton Conductivity Stability*

Proton conductivity stability of SPI membrane is also another important factor affecting membrane performance. In the case of *p*BAPBDS-based SPI membranes, no appreciable change in proton conductivity with aging was observed in the whole range of RH even after the aging in water at 100 °C for 300 h and in water or 100% RH vapor at 130 °C for 96–192 h, although the weight loss and sulfur loss up to 10 wt % and 9 mol %, respectively, took place (see Tables III and IV). This is probably because the sulfonic acid content in membrane after the aging might not decrease so large as the sulfur loss. Thus, the *p*BAPBDS-based SPI membranes showed the high proton conductivity stability.

On the other hand, in the case of 2,2′-(or 3,3′)-BSPB-based SPI membranes, the proton conductivities decreased with the aging at 100 or 130 °C. The decrease in $\sigma$ significantly depended on the RH. As shown in Table III, The reduction in $\sigma$ was only 20% and rather small in water, but with decreasing RH the reduction in $\sigma$ increased significantly up to 85–90% at 50% RH. As mentioned above, a large part of the sulfur loss was due to the cleavage of sulfopropoxy group rather than the hydrolysis of imide ring followed by dissolution of sulfonated diamine residue, resulting in an appreciable decrease in the sulfonic acid content in membrane. The actual decrease in IEC might be not so large and affect slightly the conductivity in water but more largely at lower RH. With the aging at 100 °C, as mentioned above, the S loss significantly varied from membrane to membrane, and the proton conductivity change also varied similarly. For NTDA-2,2′-BSPB/BAPB (2/1)-s (**M7**) and NTDA-2,2′-BSPB/BAPPS (2/1) (**M8**), of which the sulfur losses were smaller, no appreciable change in $\sigma$ was observed in the whole range of RH even after the aging for 300 h. On the other hand, for NTDA-2,2′(or 3,3′)-BSPB/BAPB (2/1) (**M6-1** and **M9-1**), of which the sulfur losses were larger, the larger decrease in $\sigma$ took place at the lower RHs, as in the case of the aging at 130 °C. Thus, the BSPB-based SPI membranes displayed rather poor proton conductivity stability especially with the aging at 130 °C. With the aging at 100 °C, some membranes showed reasonably high proton conductivity stability. The BSPB-based SPI membranes have the microphase-separated structure,[34] and rather small difference in membrane morphology might play a large role on their proton conductivity stability.

The 2,2′-BSPOB- and 3,3′-BSPOB-based SPIs also displayed no reduction in $\sigma$ after aging in water at 130 °C for 192 and 300 h, indicating the high proton conductivity stability as well as the stability of phenoxy side groups.

From the view points of mechanical stability, hydrolytic stability and proton conductivity stability, BAPBDS-based B/C-SPI and BSPOB-based SPI membranes displayed the water stability of 200 h for the accelerated test at 130 °C, and were reasonably considered to have the water stability as long as 300 h or more. BSPOB-based co-SPI membrane actually displayed the high water stability of 300 h, and was evaluated to have the water stability of 500 h or more. Assuming the activation energy of hydrolytic degradation of 100 kJ/mol, the water stability of 300 h at 130 °C corresponds to 3300 and 20000 h at 100 and 80 °C, respectively. Taking the operational humidity condition of 60–80% RH in PEFC applications, their water stability would be improved more. Therefore, some SPI membranes have the reasonably high water stability for PEFC application at 80 °C and also at 90–100 °C with further improvement. The SPI membranes dealt here have no problem as for the water stability for DMFC application below 80 °C.

## PHYSICAL PROPERTIES OF SPI MEMBRANES

The physical properties of SPI membranes include thermal properties, water vapor sorption, water uptake and dimensional change, as well as membrane morphology.

*Thermal Properties of SPI Membranes*

Thermal stability of SPIs was investigated by TG-MS measurement. The weight loss starting from 250–350 °C is attributed to the decomposition of the sulfonic acid groups judging from the evolution of sulfur monoxide and sulfur dioxide.[26,33] The BAPBDS-based SPIs generally displayed decomposition temperature of sulfonic acid groups around 300 °C. In the case of 2,2′- or 3,3′-BSPB-based SPIs, the evolution of propane and propylene were also observed around 250 °C, indicating the decomposition of sulfopropoxy

side groups. The decomposition temperatures of BSPB-based SPIs were in the range of 232 to 256 °C, which was lower than those of the BAPBDS-based SPIs, indicating lower thermal stability of the sulfopropoxy groups. The side-chain-type SPIs bearing aromatic sulfonated carbonyl side groups from BAPSBPS (**M15**) is noted to display high decomposition temperature of 350 °C, indicating higher thermal stability of the sulfonic acid groups bonding to a phenyl ring with lower electron density. DSC curves revealed that no clear glass transition temperature could be observed for the sulfonated polyimides.

*Membrane Morphology*

The microstructure of SPI membranes stained with silver ion was investigated by transmission electron microscopy (TEM) analysis. The cross section micrographs of NTDA-BAPBDS, NTDA-2,2′-BSPB, and NTDA-2,2′-BSPB/BAPB (2/1) membranes are shown in Figure 8. The darker regions represent localized hydrophilic ionic domains and the lighter parts refer to hydrophobic moieties. It was found that the side-chain-type of both (a) homo-SPI and (b) co-SPI membranes derived from 2,2′-BSPB had clear microphase-separated structures. The ionic domains with an average size of about 5 nm were observed for these SPI membranes. However, the connecting behavior of hydrophilic domains was somewhat different. In the case of homo-SPIs, the ionic domains seemed to be connected to form ionic pathways or channels that are favorable for water keeping and proton transport, whereas the formation of such kind of ionic channels was relatively poor in co-SPI samples. This means that the homo-SPI with higher IEC is more favorable to form ionic conducting channels compared with the corresponding co-SPI membrane. On the other hand, such kind of clear microphase-separated structure was not observed for the main-chain-type SPI membranes, even for the homo-SPI membrane, as can be seen in Figure 8c.

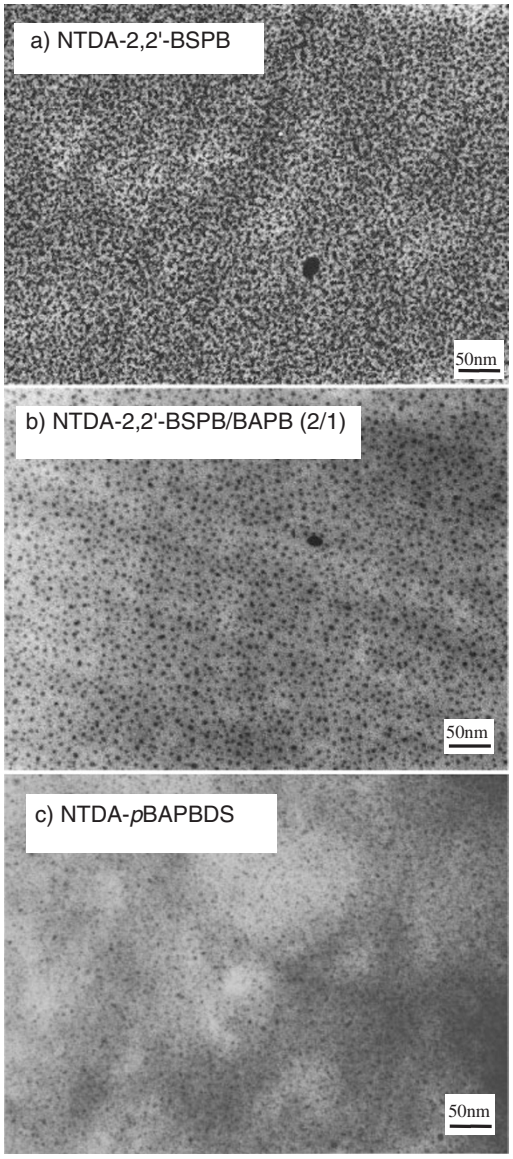


**Figure 8.** TEM images of SPI membranes in silver salt form (cross-section).

*Water Vapor Sorption Isotherm*

The water vapor sorption isotherms in a form of the number of sorbed water molecules per sulfonic acid group, $\lambda$, of typical SPIs and Nafion 117 are shown in Figure 9. With an increase in water vapor activity ($a_w$), the water vapor sorption increased sigmoidally. It is interesting that the $\lambda$–$a_w$ isotherm of the main-chain-type SPI such as **M2** was similar or close to that of Nafion 117 rather than those of the side-chain-type SPIs. The SPIs with aromatic side chains (**M10**, **M15**)

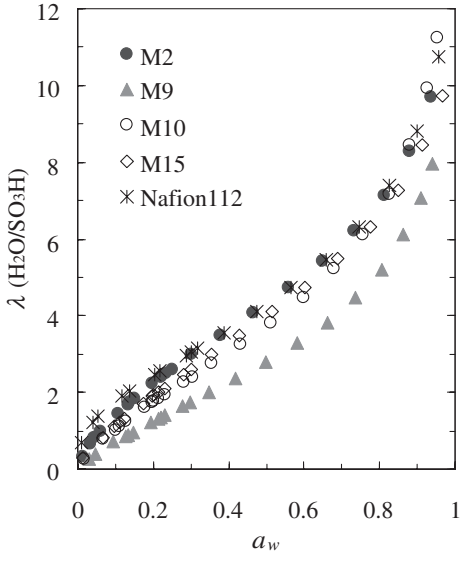


**Figure 9.** Water vapor sorption isotherms of SPI membranes and Nafion 112 at 60 °C.

displayed identical sorption behaviors in the whole $a_w$ range. They showed similar values to those of main-chain-type SPI of **M2** and Nafion 112 at high water vapor activity level ($a_w > 0.7$) but smaller ones at lower $a_w$ range. It is noted that the $\lambda$–$a_w$ isotherm of another co-SPI membrane with aliphatic side groups (**M9**) was quite different from those of the former mentioned. That is, it displayed much lower $\lambda$ values in the whole $a_w$ range. This means apparently much lower capacities of Langmuir sorption sites based on sulfonic acid groups for the aliphatic side-chain-type SPIs. However, its $\lambda$ values increased significantly with an increase in $a_w$ in the range of $a_w > 0.9$, probably due to larger molecular relaxation of polymer chains.

*Water Uptake and Membrane Swelling*

Water uptake and dimensional change of NTDA-based SPI membranes are summarized in Table II. **M2**–**M4** and **M6**–**M9** are linear co-SPIs from *p*BAPBDS and 2,2′- or 3,3′-BSPB, respectively. **M10**–**M15** are linear SPIs from aromatic side group sulfonated diamines. **M5** is a linear co-SPI from BDSA, which was used for comparison. **M16**–**M17** and **M18**–**M19** are B/C-SPIs from *p*BAPBDS and 2,2′- or 3,3′-BSPB, respectively.

Generally, water uptake is mainly dependent on IEC. Higher IEC usually leads to larger water uptake as well as larger dimensional change of membrane, and vise versa. However, there are also some exceptions resulting from the difference in polymer structure, configuration or membrane morphology. As shown in Table II, most of the SPIs displayed significantly anisotropic membrane swelling except for **M13** and **M14**, of which bearing long and bulky side groups. The dimensional change in thickness direction was much larger than that in plane. The side-chain-type SPIs generally had much larger anisotropy in membrane swelling than the main-chain-type ones. The strong anisotropic membrane swelling indicates the presence of anisotropic morphology with some degree of in-plane orientation of polyimide polymer chains in these SPI membranes. It is noted that there are some differences in viscosity, water uptake and dimensional change values between the SPI membranes with the same chemical composition but prepared in different batches under the similar conditions. For example, as shown in Table II, the membranes of **M2-1**–**M2-3** showed different water uptake and dimensional change. Similar phenomenon was also observed for **M6**. It seemed that some slight difference in high-order structure and molecular weight of SPI and membrane casting conditions resulted in a slight difference in membrane morphology or microstructure, leading to large variations in water uptake and membrane swelling. B/C-SPIs showed reduced water uptake and decreased dimensional change compared with the uncrosslinkded ones with similar IEC values.

## PROTON CONDUCTIVITY

Proton conductivity is one of the most important factors that strongly affect fuel cell performance. It is usually dependent on the IEC, water uptake, acidity of sulfonic acid group and membrane morphology of the polyelectrolytes. Larger IEC (corresponds to larger water uptake), higher acidity of sulfonic acid group (corresponds to easy dissociation of proton), and better microphase-separation in membrane morphology generally lead to high conducting performance.

Water volume fraction, $C$, was calculated based on the water uptake and density of dry membrane under the assumption of the additive law of volume of water and polymer. Figure 10 shows the relationship in the form of $\log \sigma$ *vs.* $\log C$ for SPI and Nafion 117 membranes. The SPIs and Nafion 117 membranes displayed the similar $\sigma$–$C$ relationship that with increasing $C$, the $\sigma$ values increased first sharply, then slowly and finally leveled off. It is suggested that the proton conduction paths are developed well enough to give high proton conductivities for these membranes equilibrated at high RHs above 90% ($C > 0.3$). Compared with Nafion 117, the higher conductivities of the SPIs in fully hydrated state are due to their higher IECs. On the other hand, in the range of lower $C$, Nafion membrane showed much higher proton conductivities than the SPIs. This is because Nafion membrane possesses high ion density clusters that have been proposed to form ion-rich channels being favorable for proton

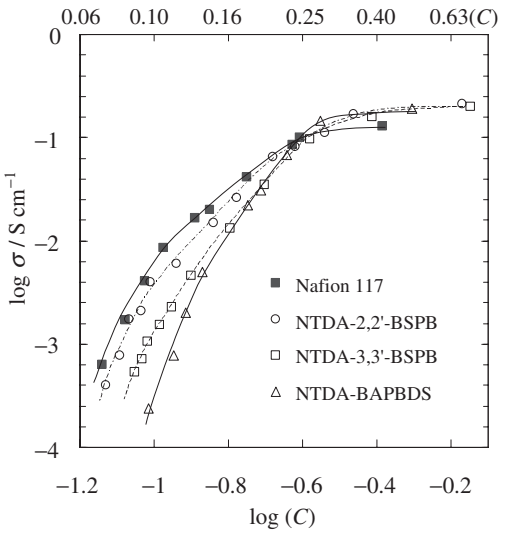


**Figure 10.** Proton conductivity of SPI membranes and Nafion 117 as a function of water volume fraction at 50 °C.

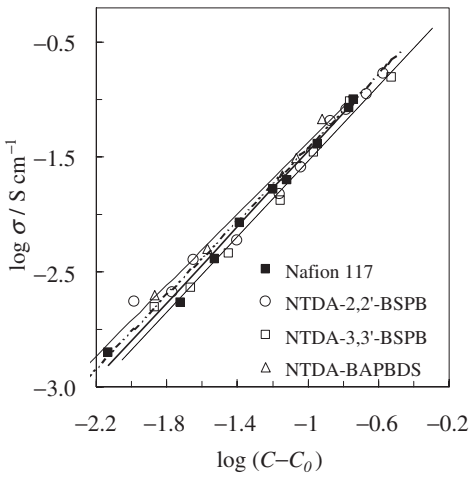


**Figure 11.** Data and best-fit lines for conductivity *vs.* water volume fraction minus percolation threshold for SPI memberanes and Nafion 117 at 50 °C.

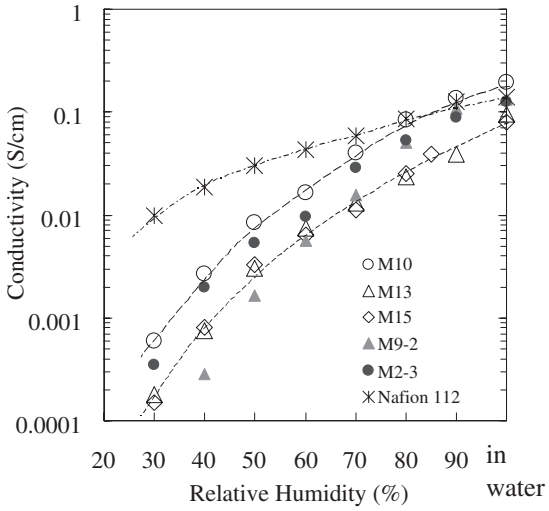


**Figure 12.** Proton conductivity at 60 °C for SPI membranes and Nafion 112 as a function of relative humidity.

transport.[43] The SPIs especially NTDA-BAPBDS needed much larger $C$ values to display the same proton conductivity as that of Nafion. This suggests the presence of a threshold water volume fraction $C_0$, below which proton conduction is impossible, and the different threshold values for these membranes.

The proton conductivity in some proton-conducting polymer membranes has been reported to obey the following percolation theory as shown in eq 1.[44–46]

$$\sigma = \sigma_0(C - C_0)^n \quad (1)$$

where $C_0$ is a threshold volume fraction required for protons to transport, $n$ is referred to as a critical exponent that controls the scaling behavior, and $\sigma_0$ is a prefactor determined by carrier number and ion transport mobility.

To test the percolation theory, $C_0$ was initially chosen as a minimum $C$ value for each membrane in Figure 10 and the calculated line of $\log\sigma$ *vs.* $\log(C - C_0)$ was best fit to the experimental data except for the datum measured in water. This procedure was repeated for various values of $C_0$ until a maximum fitting of the calculated and the experimental data was achieved. The experimental data and best-fit line for SPI membranes and Nafion 117 are shown in Figure 11. The percolation thresholds, $C_0$, of Nafion 117, NTDA-BSPB and NTDA-BAPBDS were 0.065, 0.075–0.090, and 0.105, respectively. Nafion 117 has a well-formed microphase-separated structure that is favorable for proton conduction, resulting in lower $C_0$ value. As mentioned above, the side-chain-type SPIs, NTDA-BSPB, also have microphase-separated structure where the ionic domains connected to each other to form proton-conducting pathways. This is likely the reason for the lower $C_0$ for NTDA-BSPB compared to NTDA-BAPBDS. As a result, the proton conductivity of SPI membranes could be explained by percolation theory in relation to the percolation thresholds.

Figure 12 shows relative humidity dependence of proton conductivity for typical co-SPI membranes and Nafion 112, at 60 °C. The SPIs cited in this plot had reasonable IEC values of 1.5–2.0 mequiv $g^{-1}$ (see Table II). The proton conductivity for SPI membranes generally displayed larger RH dependence than that for Nafion 112. At lower RHs below 60%, the $\sigma$ values of SPI membranes were much lower than those of Nafion. However, the deviation in proton conductivity became smaller with an increase in RH. At high RHs above 80%, the SPIs showed comparable $\sigma$ values to Nafion 112. As mentioned above, Nafion is well known to be a super acid and has a good microphase-separation structure composed of hydrophilic ionic domain (ionic cluster size ~5 nm) and hydrophobic moiety, which may be the reason of high proton conductivity even at lower RH. At higher RHs, IEC seemed to play a more important role on proton conductivity. That is why the deviation in proton conductivity between Nafion and SPIs became smaller with increasing RH, since SPIs had larger IECs.

As shown in Figure 12, SPIs of **M10** and **M2** with larger IECs of 1.8–1.9 mequiv $g^{-1}$ displayed higher proton conductivities than other SPIs in the whole RH range. It is surprise that the membrane of **M9** showed lower $\sigma$ values especially at lower RHs, although with a higher IEC of about 2.0 mequiv $g^{-1}$. This maybe explained by the much smaller water uptake values in $\lambda$ of **M9**, as shown in Figure 9, compared with other SPIs. With lower IEC values, **M13** and **M15** displayed identical conducting performance, which was comparable to that of **M9**.

It should be mentioned that some of co-SPI membranes with same chemical composition but in differ-

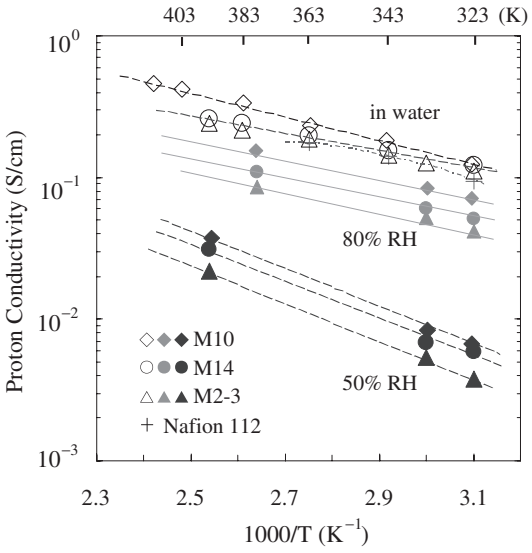


**Figure 13.** Temperature dependence of proton conductivity for SPI membranes and Nafion 112 at different relative humidities.

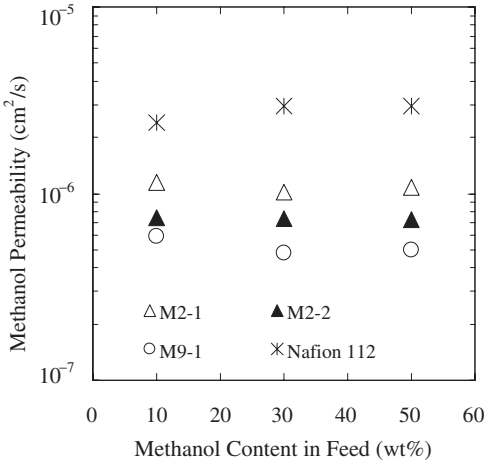


**Figure 14.** Feed composition dependence of methanol permeability for co-SPIs and Nafion 112 membranes at 30 °C.

ent batches, such as **M6** and **M9**, displayed different conducting behaviors.[34] The data can also be seen in Table II. Since the side-chain-type SPIs had microphase-separated structure, the slight difference in membrane morphology of the same kind of SPI membranes may affect the conducting behavior more or less, especially at lower RH range.

Figure 13 shows temperature dependence of proton conductivity for typical SPI membranes and Nafion 112 at different RHs. All the membranes displayed increased $\sigma$ values with an increase in temperature. The SPIs of **M10**, **M14** and **M2** generally displayed high conductivities at temperatures above 100 °C. At fully hydrated state, those three membranes with IEC values of 1.8–2.0 mequiv g$^{-1}$ showed conducting performance similar to or slightly higher than that of Nafion 112. At 120 °C, **M14** and **M2** displayed proton conductivities of 0.2–0.3 S/cm and **M10** exhibited a high $\sigma$ value of nearly 0.5 S/cm at 140 °C. At a lower RH of 50%, raising temperature led to much more significant increase in proton conductivity. At 120 °C and 50% RH, most of the SPIs displayed reasonable high $\sigma$ values of 0.02–0.04 S/cm, indicating high conducting performance under low moisture condition. The proton conductivity of SPI membranes showed an Arrhenius-type temperature dependence. The activation energy of $\sigma$, $\Delta E_a$ values for SPI membranes in water were 9–12 kJ/mol, which were similar to those reported for Nafion 117 ($\Delta E_a$ = 9–13 kJ/mol),[46] sulfonated polysulfones (10–12 kJ/mol)[47] and sulfonated polystyrene membranes (12 kJ/mol).[48] The SPI membranes displayed larger activation energies at lower RHs. At 50% RH, the $\Delta E_a$ values were tested to be in the range of 20–40 kJ/mol.

## METHANOL PERMEATION BEHAVIOR

Methanol is a more attractive fuel than hydrogen because of its much higher energy density, low cost, and ease of handle, store and transport.[49,50] A major problem existed in a DMFC is the so called "methanol crossover". That is, methanol can cross through the PEM from the anode to the cathode *via* physical diffusion and electro-osmotic drag (by protons). Such crossover not only results in a waste of fuel, but also lowers the cell performance. The methanol crossing over will be oxidized at the cathode and such an oxidation reaction lowers the cathode potential and also consumes some cathode reactant. If a reaction intermediate, such as carbon monoxide adsorbs on to the catalyst surface, the cathode will be poisoned too, which further lowers cell performance. The effect of methanol crossover or methanol permeation has attracted much attention throughout the world.[51,52]

The methanol permeation behavior was investigated for typical co-SPI membranes. Figure 14 shows feed composition dependence of methanol permeability ($P_M$) for co-SPIs and Nafion 112 membranes at 30 °C. With an increase in methanol content in feed ($x_M$) from 10 wt % up to 50 wt %, the $P_M$ for Nafion 112 slightly increased from $2.4 \times 10^{-6}$ cm$^2$/s up to $3.0 \times 10^{-6}$ cm$^2$/s. On the other hand, the $P_M$ values for co-SPI membranes were much lower than those of Nafion 112 and hardly depended on the methanol content in feed.

Figure 15 shows temperature dependence of $P_M$ for co-SPIs and Nafion 112 membranes at $x_M$ of 30 or 10 wt %. The activation energy of $P_M$ ($\Delta E_{aP}$) for Nafion 112 was about 22 KJ/mol, which was close to the values reported in literature (18 and 22.4 KJ/mol at $x_M$ of 6 and 50 wt %, respectively).[52,53] The $\Delta E_{aP}$ values for co-SPI membranes were 25–26 KJ/mol, which were

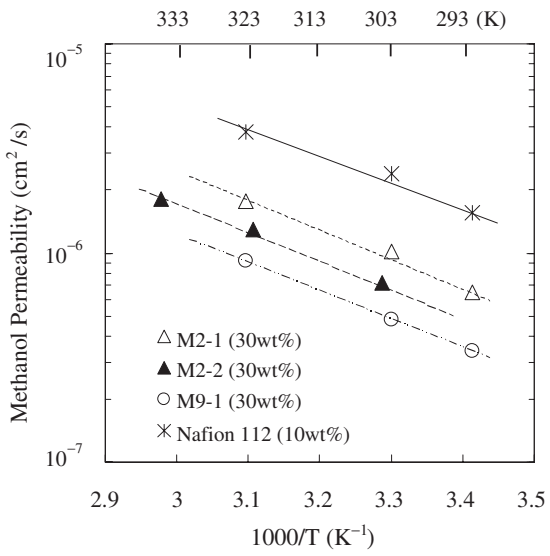


**Figure 15.** Temperature dependence of methanol permeability for co-SPI and Nafion 112 membranes at $x_M$ of 10 or 30 wt %.

comparable to those for Nafion membranes. A slightly smaller $\Delta E_{aP}$ value of 18 kJ/mol have been observed for IonClad R-1010 and R-4010 membranes,[52] whereas larger values of 41 and 37 KJ/mol for C/S-PPP and S-SIBS membranes, respectively.[53,54]

The $P_M$ values are summarized in Table V. Nafion 112 showed a high $P_M$ value of $2.4 \times 10^{-6}$ cm$^2$/s at $x_M$ of 10 wt % and 30 °C, which was in agreement with the values reported in literature (2.3 and $2.6 \times 10^{-6}$ cm$^2$/s) at the same $x_M$ and room temperature.[55,56] The co-SPIs showed more than two times smaller $P_M$ values than Nafion 112. The ratios of $\sigma$ to $P_M$, $\phi = \sigma/P_M$, are also listed in Table V. The ratio $\phi$ is an effective parameter evaluating the membrane performance in a DMFC system. With an increase in temperature, the $\phi$ decreased as a result of the larger activation energy of methanol permeation than that of proton conductivity. The $\phi$ values of Nafion 112 membrane were 3–4 $\times 10^4$ S cm$^{-3}$ s at 30 and 50 °C. As shown in Table V, the co-SPI membranes displayed 2–4 times larger $\phi$ values than Nafion 112.

Nafion is known to have well-developed microphase-separation and proton conducting channels or connected ionic domains, which give high proton conductivity and also high methanol permeability. The co-SPI membranes have much lower methanol permeability and comparable proton conductivity in water, compared with Nafion. This is likely explained based on both the difference in morphology between Nafion and co-SPI membranes and the difference in the transport mechanism between proton conduction and methanol permeation.

Table VI shows comparison of the $\sigma$, $P_M$ and $\phi$ values among PEMs reported in literature and SPIs. Fluorinated ionomer membranes (IonClad R-1010 and R-4010) showed good performance of high $\sigma$ and $\phi$ values.[52] The C/S-PPP membrane with IEC of 1.07 meq/g has been reported to have high $\phi$ values of 24 $\times$ and $8.4 \times 10^4$ S cm$^{-3}$ s at 25 and 80 °C, respectively.[53] The SPI membrane derived from 3,3′,4,4′-bezophenonetetracarboxylic dianhydride (BTDA), BDSA and 4,4′-oxydianiline (ODA) with IEC of 1.75 mequiv g$^{-1}$ has also been reported to have an extremely high $\phi$ value of $56 \times 10^4$ S cm$^{-3}$ s at room temperature.[57] In these two membranes, the high $\phi$ values were due to the much smaller $P_M$ values than for Nafion membranes, whereas the $\sigma$ values were about two times smaller. Such high $\phi$ values were not observed for the present co-SPI membranes. However, it is noted that some co-SPI membranes showed high proton conductivities comparable to Nafion 112 and simultaneously 3–4 times lower methanol permeabilities than Nafion and as a result, fairly high $\phi$ values of 13–18 and 10–13 $\times 10^4$ S cm$^{-3}$ s at 30 and 50 °C, respectively.[58] This indicates that the co-SPI membranes have high potential for DMFC application.

## FUEL CELL PERFORMANCE

### *Polymer Electrolyte Fuel Cell*

Membrane-electrode assemblies (MEAs) were prepared by hot-pressing electrode/membrane/electrode

**Table V.** Proton conductivity ($\sigma$), methanol permeability ($P_M$) and the ratios ($\phi$) of SPI membranes

| SPIs | $\sigma$ (mS/cm)[a] | | $P_M$ ($10^{-6}$ cm$^2$/s)[b] | | $\phi$ ($10^4$ S cm$^{-3}$ s)[b] | |
|---|---|---|---|---|---|---|
| | 30 °C | 50 °C | 30 °C | 50 °C | 30 °C | 50 °C |
| | | | 10% (30%) | 10% (30%) | 10% (30%) | 10% (30%) |
| M2-1 | 91 | 124 | 1.15 (1.02) | 1.66 (1.77) | 7.9 (8.9) | 7.5 (7.0) |
| M2-2 | 72 | 102 | 0.75 (0.73) | (1.31) | 9.6 (10) | (7.8) |
| M6-0 | 52 | 63 | 0.34 (0.66) | 0.51 | 15 (7.9) | 12 |
| M6-1 | 80 | 107 | (1.00) | — | (8.0) | — |
| M8 | 43 | 54 | 0.41 (0.32) | 0.47 | 10 (13) | 11 |
| M9 | 82 | 118 | 0.62 (0.48) | 1.04 (0.92) | 13 (17) | 11 (13) |
| Nafion 112 | 10 | 130 | 2.4 (3.0) | 3.8 (4.0) | 4.2 (3.3) | 3.4 (3.3) |

[a]Measured in water. [b]$x_M$ = 10 and 30 wt %. The data in parenthesis refer to the values at $x_M$ of 30 wt %.

**Table VI.** Comparison of $P_M$, $\sigma$ and $\phi$ among PEMs

| PEMs[a] | Thickness (μm) | IEC (meq/g) | WU (wt %) | Conditions[b] (°C) | Conditions[b] (wt %) | $P_M$ ($10^{-6}$ cm$^2$/s) | $\sigma$[c] ($10^{-2}$ S/cm) | $\phi$ ($10^4$ S cm$^{-3}$ s) | Ref. |
|---|---|---|---|---|---|---|---|---|---|
| M2-1 | 32 | 1.89 | 45 | 30 | 30 | 0.73 | 7.2 | 10 | 58 |
| | | | | 63 | 30 | 1.81 | 12.1 | 6.7 | 58 |
| M9-2 | 24 | 2.02 | 64 | 30 | 30 | 0.48 | 8.2 | 17 | 58 |
| | | | | 50 | 30 | 0.92 | 11.8 | 13 | 58 |
| Nafion 112 | 55 | 0.91 | 30 | 30 | 10 | 2.4 | 10 | 4.2 | 58 |
| R-1010 | 36 | 1.2 | — | 60 | 6 | 1.37 | 14.6 | 10.7 | 52 |
| R-4010 | 63 | 1.5 | — | 60 | 6 | 0.94 | 13.2 | 14 | 52 |
| C/S-PPP | 183 | 1.07 | 38 | 25 | 10 | 0.145 | 4.5 | 24 | 53 |
| | | | | 80 | 10 | 1.54 | 13 | 8.4 | 53 |
| BTDA-BDSA/ODA | 85 | 1.75 | 16 | 25 | 15 | 0.073 | 4.1 | 56 | 57 |
| Sulfonated polystyrene | 338 | 1.41 | 44 | 22 | 6 | 0.52 | 5.0 | 9.6 | 48 |
| | | | | 60 | 6 | 1.19 | 11.9 | 7.2 | 48 |
| S-SIBS | 200–300 | 0.97 | — | 25 | 6 | 0.139 | 2.47 | 18 | 54 |
| | | | | 80 | 6 | 1.46 | 8.3 | 5.7 | 54 |

[a]R-1010 and R-4010: poly(styrenesulfonic acid) side chains grafted to a perflurorinated polymeric backbone; C/S-PPP: crosslinked and sulfonated poly(phenoxy)phosphazene; S-SIBS: sulfonated poly(styrene-isobutylene-styrene). [b]Temperature and feed cocentration of methanol for measurement of $P_M$. [c]Measured in water at the same temperature for $P_M$.

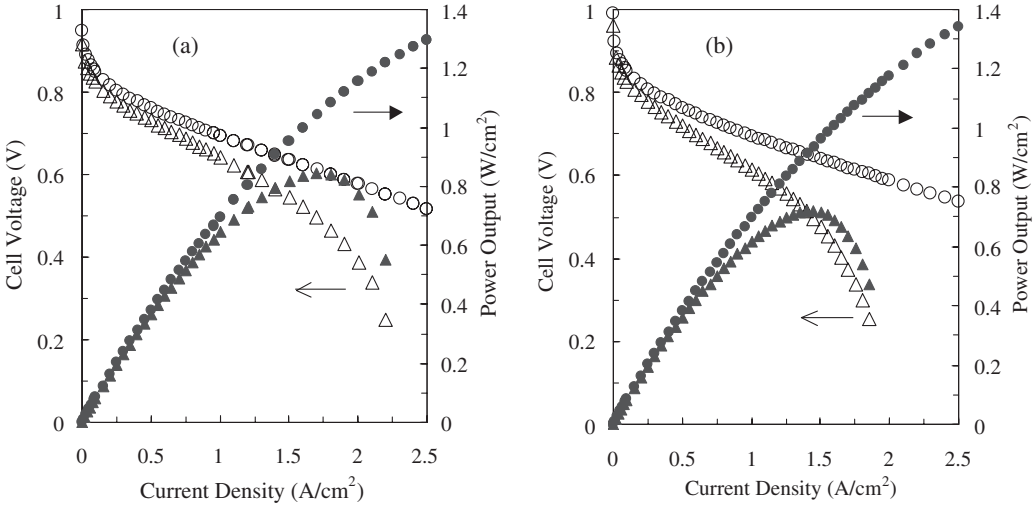


**Figure 16.** PEFC performances at 90 °C and 0.3 MPa for (a) Nafion 112 (55 μm) and (b) co-SPI of NTDA-2,2′-BSPB/BAPB (2/1) (33 μm) supplied with $O_2$ (○● 100 mL/min) and air (△▲ 500 mL/min) at cathode. (Pt (Pt/C: 30 wt %): 0.5 mg/cm$^2$, Humidifier temperature: 88 °C for $H_2$, 85 °C for $O_2$ and air).

sandwiches at 135 °C for 10 min under 60 kg/cm$^2$. The effective electrode area was 5 cm$^2$. Figures 16a and 16b show the performances of PEFCs with Nafion 112 and co-SPI membranes. The open circuit voltage (OCV) and cell voltage at current density of 1.0 A cm$^{-2}$ ($V_1$) are summarized in Table VII, including the data for PEFCs with other SPI membranes. The complex impedance spectra of cell were measured at different dc voltages. Assuming a simple equivalent circuit, membrane resistance ($R_m$) and reaction resistance at electrodes ($R_{el}$) were evaluated from the impedance spectra.[59] The $R_m$ and $R_{el}$ values at 1.0 V are listed in Table VII. The lower $R_{el}$ values indicate the good contact of MEAs, which is essential for the high performance of fuel cells. In the case of oxygen supply in the cathode, the SPI membranes displayed the high PEFC performances comparable to those of Nafion 112. On the other hand, in the case of air supply, the SPI membranes displayed slightly lower PEFC performances because of slightly larger $R_{el}$ values. This implies the presence of a little larger resistance for gas diffusion in cathode catalyst layer, and the MEA preparation process should be improved.

The $R_m$ was hardly dependent of dc voltage, and was attributed mainly to conduction resistance of membrane except for too thin membranes. The proton conductivity in thickness direction of membrane ($\sigma_\perp$) was calculated from $R_m$ and is listed in Table VII.

**Table VII.** Properties of PEFCs with SPI and Nafion 112 membranes operated at 90 °C[a]

| SPIs | Pt/C loading (wt %) | Thickness (μm) | OCV (mV) | $V_l$ (mV) | $R_m$ (mΩ) | $R_{el}$ (mΩ) | $\sigma_\perp$ (mS/cm) | $\sigma_{//}$ (mS/cm) |
|---|---|---|---|---|---|---|---|---|
| M2 (88/85) | 20 | 23 | 948 | 685 | 14 | 16 | (32) | 130 |
| (85/82) | 20 | 23 | 955 | 696 | 14 | 16 | (32) | 130 |
| (80/80) | 20 | 23 | 951 | 672 | 15 | 17 | (31) | 130 |
| M19 | 20 | 40 | 996 | 685 | 18 | 20 | 43 | 150 |
| Nafion 112 | 20 | 55 | 982 | 658 | 15 | 15 | 74 | 140 |
| M2 | 30 | 38 | 987 | 716 | 14 | 13 | 54 | 130 |
| M6 $O_2$ | 30 | 33 | 978 | 708 | 14 | 14 | 46 | 140 |
| Air | 30 | 26 | 963 | 616 | 14 | 41 | (38) | 140 |
| M16 $O_2$ | 30 | 35 | 981 | 706 | 12 | 13 | 59 | 140 |
| Air | 30 | 35 | 956 | 585 | 11 | 79 | 62 | 140 |
| Nafion 112 $O_2$ | 30 | 55 | 963 | 688 | 17 | 12 | 65 | 140 |
| Air | 30 | 55 | 916 | 643 | 17 | 35 | 66 | 140 |

[a]Conditions are the same as mentioned in Figure 16 or Figure 17.

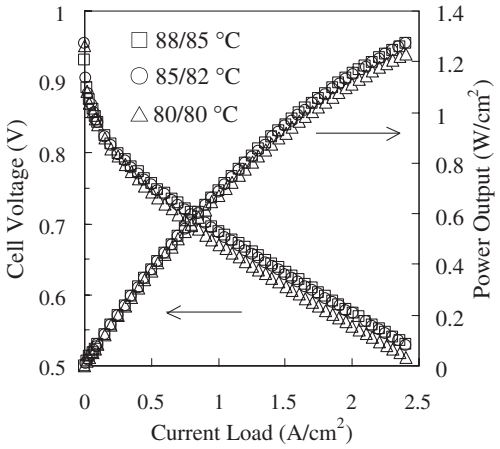


**Figure 17.** Effect of humidifier temperature on PEFC performance for NTDA-BAPBDS/BAPB (2/1) 34 (23 μm). Cell: 90 °C, 0.3 MPa, $H_2$: 150 mL/min, $O_2$: 100 mL/min.

Judging from the operational conditions of PEFCs, the data correspond to the $\sigma_\perp$ values at 90 °C and 90% RH. For comparison, the conductivities in plane direction of membranes (referred as "$\sigma_{//}$" here after) at the same conditions were evaluated from the data at 50 °C and 90% RH using the activation energy of 10 kJ/mol,[60] as shown in Table VII. The $\sigma_\perp$ values were about 30–50% as those of the $\sigma_{//}$ ones. It is noted that the anisotropy of proton conductivity is slightly larger for the BSPB-based SPIs of **M6** and **M19**, with the larger anisotropy of membrane swelling, than for the BAPBDS-based SPIs of **M2** and **M16**.

Figure 17 shows effect of humidifier temperature on PEFC performance for NTDA-BAPBDS/BAPB (2/1) membrane.[59] When the temperature of $H_2/O_2$ humidifiers decreased from 88/85 °C (corresponding to 93/84% RH) to 80/80 °C (70/70% RH), a slight decrease in cell voltage, for example, by about 20 mV at a current density of 1.0 A/cm$^2$ was observed. Judging from the large dependence of proton conductivity on RH, this rather small effect implies effective back diffusion of water formed at the cathode into the membrane bulk. This is due to not only thinner membrane but also the water transport behavior characteristic to SPI membrane, that is, the water transport through SPI membrane is not controlled by electro-osmotic drag but by diffusion according to the activity difference as mentioned below.

A short-term stability test was carried out for a cell with the SPI membrane under the same conditions as in Figure 16.[61] The test cell kept a cell voltage of 0.75 V with a current density of 0.5 A/cm$^2$ for 300 h. The degradation rate was about 20 μV/h. Judging from the water stability test mentioned above, the SPI membranes have high potential for PEFC applications working at 80 °C.

*Direct Methanol Fuel Cell*

DMFCs are suited for portable devices or transportation applications owing to their high energy density at low operating temperatures and the ease of handling a liquid fuel.[50] However, the methanol crossover across MEA impedes the improvement of DMFC performance, as has been reported for Nafion.[51] There have been much attention for development of alternative membranes that have lower methanol permeability with minimal loss of proton conductivity.[62–64] The SPI membranes dealt in this review have high tolerance against methanol. They don't swell in methanol rather than in water. This is quite different from other sulfonated aromatic polymers such as sulfonated poly(arylene ethers). Although having reasonably high proton conductivities due to higher IECs, the SPI membranes have lower methanol permeabilities even at high methanol concentrations. Thus, they have high potential for DMFC applications.[65]

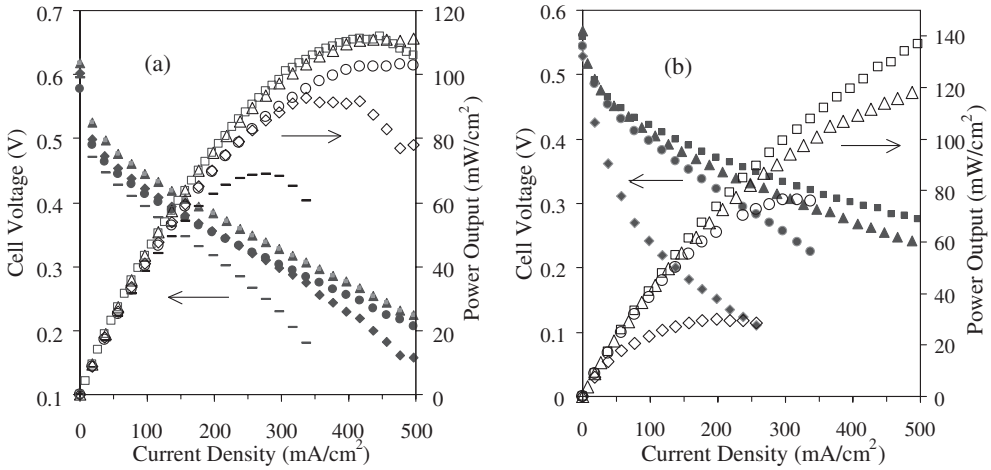


**Figure 18.** Effects of MeOH concentration on DMFC performance for (a) NTDA-BAPBDS/TAPB (6/1) (45 μm) and (b) Nafion 112. (effective electrode area: 5 cm$^2$; 2.2 mg/cm$^2$ Pt-Ru for anode and 1.8 mg/cm$^2$ Pt for cathode); (□■: 5%, △▲: 10%, ○●: 20%, ◇◆: 30%, –: 50 wt %) MeOH: 1 mL/min, $O_2$: 150 mL/min; 60 °C; atmospheric pressure.

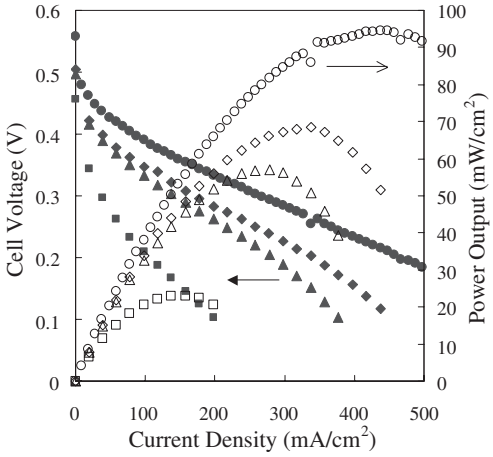


**Figure 19.** Effects of cathode gas and its flow rate on DMFC performance for NTDA-BAPBDS/BAPB (2/1) (38 μm) at 60 °C. (30 wt % MeOH, ○●: $O_2$: 150 mL/min, ◇◆: air: 750 mL/min, △▲: air: 450 mL/min, □■: air: 150 mL/min)

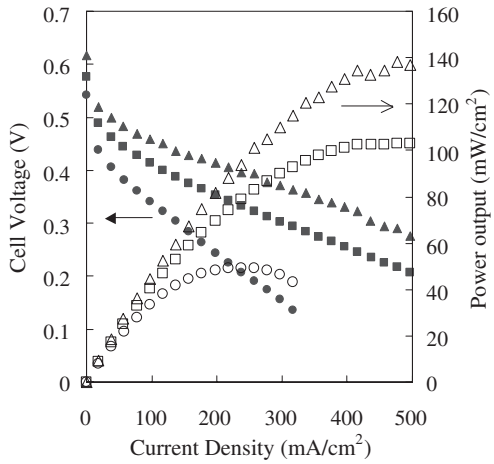


**Figure 20.** Temperature dependence of DMFC performance for NTDA-BAPBDS/TAPB (6/1) (45 μm). 20 wt % MeOH, $O_2$: 150 mL/min. (○●: 40 °C, □■: 60 °C, △▲: 80 °C)

Figures 18a and 18b show the performances for DMFCs with NTDA-BAPBDS/TAPB (6/1) (**M16**) and Nafion 112, respectively, supplied with methanol concentration of 5–50 wt %, at 60 °C. With 5 wt % methanol, Nafion 112 displayed a high maximum power output $W_{max}$ of about 140 mW cm$^{-2}$ at 500 mA/cm$^{-2}$, which was 20% higher than that for the SPI. With an increase in methanol concentration, the fuel cell performance decreased slightly for the SPI but largely for Nafion 112. As a result, at 30 wt % methanol, the SPI kept the high $W_{max}$ of 92 mW cm$^{-2}$, which was 3 times larger than that for Nafion 112. At a methanol concentration of 50 wt %, the DMFC with Nafion 112 did not work stably, whereas the DMFC with the SPI still kept reasonably high $W_{max}$ of 69 mW cm$^{-2}$.

Figure 19 shows effects of cathode gas and its flow rate on DMFC performance for NTDA-BAPBDS/BAPB (2/1). When oxygen was supplied into cathode, the DMFC performance hardly depended on the flow rate above 30 mL/min. On the other hand, in the case of air supply, the DMFC performance was much lower and significantly increased with increasing air flow rate. At 750 mL/min, the $W_{max}$ was 68 mW cm$^{-2}$ at 30 wt % methanol, which was 30% lower than that for oxygen supply. The reduction in DMFC performance with air supply was larger for Nafion 112 than for SPI membranes especially at higher methanol concentration. For Nafion 112, the $W_{max}$ was of 82 mW cm$^{-2}$ at 10 wt % methanol, which was similar to that for the SPI membrane at 20 wt % methanol.

Figure 20 shows temperature dependence of DMFC performance for NTDA-BAPBDS/TAPB (6/1) (**M16**). Even at 20 wt % methanol, OCV and $W_{max}$ increased significantly with increasing temperature up to 80 °C.

This indicates that, in the case of DMFCs with SPIs, the advantageous effect of higher temperature on the electrode reaction overcame its adverse effect on methanol crossover, which was different from the case of Nafion 112.

Figures 21a and 21b show methanol and water crossover through Nafion 115 and SPI membranes measured during DMFC operation. In Figure 21a, for Nafion 115, the water flux $q_W$ increased significantly with increasing load current density due to the increasing contribution of electro-osmotic drag of proton migration. From the slope of the line in the current range above 200 mA cm$^{-2}$, the water electro-osmotic drag coefficient for Nafion 115 was evaluated as 2.4 $H_2O/H^+$, which was close to the literature values of 2.5–3.3 $H_2O/H^+$ at lower methanol concentrations less than 3 wt %.[66,67] On the other hand, for SPI membrane, the $q_W$ slightly decreased with increasing current density, indicating that the water flux was controlled by the diffusion but not by the electro-osmosis under the present conditions. This is due to the difference in membrane morphology. The SPI membranes have no clear hydrophilic ionic channel structure as considered in Nafion membranes and have less loosely bonded and/or free water than Nafion membranes. The similar water crossover behavior has been reported for poly(arylene ethers).[67] In Figure 21b at a constant current density of 200 mA cm$^{-2}$, for Nafion 115, the $q_W$ hardly changed, because it was controlled by the electro-osmosis. On the other hand, for SPI membrane, the $q_W$ decreased largely with increasing methanol concentration (or with decreasing water concentration) and became negative at 50 wt % methanol. This was due to the decrease in driving force of water diffusion.

In Figure 21a, for Nafion 115, the methanol flux $q_M$ increased largely with increasing current density. This indicates that an increase in the water flux due to the electro-osmosis caused a fairly large increase in the methanol flux. On the other hand, for SPI membrane, the $q_M$ hardly changed with the current density. In Figure 21b, with increasing methanol concentration at a constant current density, the $q_M$ increased slightly linearly and sublinearly for Nafion and SPI membranes, respectively. This is due to the difference in membrane swelling in higher methanol concentration. The methanol permeation coefficient $P_M$ values calculated from the $q_M$ values which are listed in Table VIII were two or three times smaller than those measured from the liquid–liquid permeation experiments mentioned above. This is because of the lower membrane swelling for DMFC operations, where the membranes at the cathode were contact with gas instead of water.

As mentioned above, the water and methanol crossover behavior is quite different between Nafion and SPI membranes. In the case of Nafion membranes, methanol crossover increases largely with increasing methanol concentration and also with increasing load current density. Methanol crossover is followed by methanol electro-oxidation on cathode, which competes with oxygen reduction on cathode, resulting in a mixed potential and a reduction of OCV[50] as well as a reduction of Faraday's efficiency (percentage of methanol utilized for electricity per methanol consumed). Furthermore, under the conditions of a higher methanol concentration and a higher load current density, the total amount of water in the cathode became much larger for Nafion than for SPI membrane, as listed in Table VIII, because of larger water crossover and larger water formation *via* oxidation of crossovered methanol. This interrupts diffusion of oxygen molecules from gas diffusion layer to catalyst layer of cathode. As a result, oxygen supply into catalyst layer is apt to become a rate-determining step, espe-

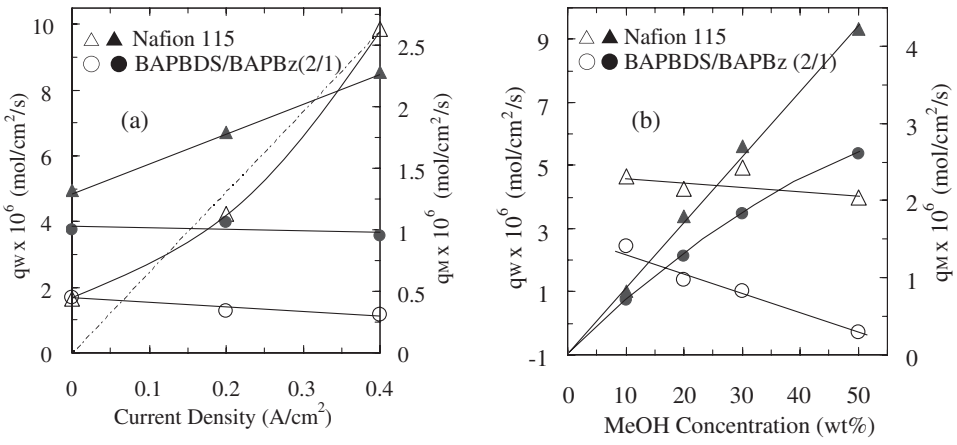


**Figure 21.** Water flux (△○) and methanol crossover (▲●) for DMFCs with Nafion 115 and NTDA-BAPBDS/BAPBz (2/1) (50 μm) membranes at 60 °C with $O_2$ of 150 mL/min humidified at 25 °C. (a) effect of current density at 20 wt % MeOH. (b) effect of methanol concentration at a current density of 200 mA/cm$^2$.

**Table VIII.** Methanol and water crossover ($q_M$, $q_W$), methanol permeability ($P_M$), total water flux in cathode exhaust ($Q_{W,C}$) and faraday' efficiency for DMFC cells

| PEMs | Current (mA/cm$^2$) | $q_M \times 10^6$ (mol/cm$^2$ s) | $P_M \times 10^6$ (cm$^2$/s) | $Q_{W,C} \times 10^6$ (mol/cm$^2$ s) | $q_W \times 10^6$ (mol/cm$^2$ s) | Faraday's efficiency (%) |
|---|---|---|---|---|---|---|
| Nafion115 | 0 | 1.32 | 2.76 | 4.9 | 1.64 | 0 |
| (130 μm) | 200 | 1.79 | 3.74 | 9.2 | 4.2 | 16 |
| | 400 | 2.28 | 4.78 | 16.4 | 9.9 | 23 |
| M3-1 | 0 | 1.00 | 0.71 | 4.2 | 1.67 | 0 |
| (44 μm) | 200 | 1.06 | 0.75 | 4.5 | 1.26 | 27 |
| | 400 | 0.95 | 0.72 | 5.1 | 1.16 | 42 |

Cell temperature: 60 °C, 20 wt % MeOH: 1 mL/min, $O_2$: 150 mL/min.

cially for the case of air supply in cathode. This causes further reduction in DMFC performance, especially of maximum output, for Nafion membranes at a higher methanol concentration and/or for air supply. In the case of SPI membranes, both the water and methanol fluxes hardly depended on load current density and they are kept at lower levels even at higher current density and higher methanol concentration. As a result, the adverse effects taken place seriously for Nafion membranes are not so serious for SPI membranes and the DMFC performance is kept at a higher level.

Although exact comparison is not suitable, the DMFC performances for SPI membranes mentioned above are higher than the literature data.[62,67,68] The SPI membranes have high potential for DMFC applications with high methanol concentration. To improve the Faraday's efficiency, the methanol crossover should be lowered to a half. At present, Nafion-bonded electrodes were employed for DMFC applications. To improve the compatibility of MEA between electrodes and membrane, SPI-bonded electrodes where SPI is employed as ionomer in catalyst layer must be developed.

## CONCLUDING REMARKS

(1) Water stability of SPI membranes was a comprehensive result of solubility property, hydrolysis stability, swelling-stress stability and membrane morphology. High IEC and good solubility behavior lead to poor water stability, and vise versa. High flexibility of polymer chain, more basic sulfonated diamine and good microphase separation lead to high water stability. The *p*BAPBDS-based co-SPIs displayed the best water stability among the main-chain-type SPI membranes. The 2,2′- or 3,3′-BSPB-based SPIs were not tolerable under aging in water at 130 °C due to the cleavage of sulfopropoxy side group. The 2,2′- or 3,3′-BSPOB-based co-SPIs with aromatic side groups and the B/C-SPI membranes kept much better mechanical properties. From the viewpoints of mechanical and conductivity properties, the water stability of the SPI membranes was more than 200–300 h in water at 130 °C, suggesting their potential as PEMs working at 80 °C and also at 90–100 °C with further improvement.

(2) Water uptake and proton conductivity of SPI membranes was determined mainly by IEC and membrane morphology. Most of the SPI membranes displayed anisotropic membrane swelling in water with much larger dimensional change in thickness than in plane because of preferable in-plain orientation of polymer chain, which was more significant for the side-chain-type SPIs than for the main-chain-type ones. Higher IEC, larger water uptake and better microphase-separation led to higher conducting performance. The proton conducting behavior of SPI membranes could be explained by means of the percolation model. Some SPI membranes displayed reasonably high conductivities at temperatures above 100 °C even at lower relative humidities.

(3) Although having reasonably high proton conductivity due to higher IEC, the SPI membranes with excellent tolerance against methanol have lower methanol permeability even at higher methanol concentrations, being different from other sulfonated aromatic polymers.

(4) The water and methanol crossover through SPI membranes under the fuel cell operation conditions is not controlled by electro-osmosis due to proton transport but by diffusion due to activity difference. This is quite different from the case of perfluorosulfonated membranes such as Nafion and results in the advantageous effects on fuel cell performance. PEFCs with SPI membranes exhibited high performances at 70–90 °C even under lower humidification conditions. DMFCs with SPI membranes displayed reasonably high performances even with higher methanol concentration (20–50 wt %) at mediate temperatures (40–80 °C).

*Acknowledgment.* This work was financially supported by NEDO (New Energy and Industrial Technology Development): Fuel cell & hydrogen technology development department, "Research and development of polymer electrolyte fuel cells", and by the Venture Business Laboratory of Yamaguchi University, Japan.

## REFERENCES

1. a) P. Costamagna and S. Srinivasan, *J. Power Sources*, **102**, 242 (2001).
   b) P. Costamagna and S. Srinivasan, *J. Power Sources*, **102**, 253 (2001).
2. V. Mehta and J. S. Cooper, *J. Power Sources*, **114**, 32 (2003).
3. O. Savadogo, *J. New Mater. Electrochem. Syst.*, **1**, 47 (1998).
4. K. A. Mauritz and R. B. Moore, *Chem. Rev.*, **104**, 4535 (2004).
5. M. Rikukawa and K. Sanui, *Prog. Polym. Sci.*, **25**, 1463 (2000).
6. J. A. Kerres, *J. Membr. Sci.*, **185**, 3 (2001).
7. K. D. Kreuer, *J. Membr. Sci.*, **185**, 29 (2001).
8. Q. Li, R. He, J. O. Jensen, and N. Bjerrum, *Chem. Mater.*, **15**, 4896 (2003).
9. M. A. Hickner, H. Ghassemi, Y. S. Kim, B. R. Einsla, and J. E. Mc-Grath, *Chem. Rev.*, **145**, 4587 (2004).
10. S. Faure, N. Cornet, G. Gebel, R. Mercier, M. Pineri, and B. Sillion, Proc. 2nd Int. Symp. New Materials for Fuel Cell and Modern Battery Systems, Eds. O. Savadogo and P. R. Roberge, Montreal, Canada, July 6–10, 1997.
11. E. Vallejo, G. Porucelly, C. Gavach, R. Mercier, and M. Pineri, *J. Membr. Sci.*, **160**, 127 (1999).
12. N. Cornet, O. Diat, G. Gebel, F. Jousse, D. Marsacq, R. Mercier, and M. Pineri, *J. New Mater. Electrochem. Syst.*, **3**, 33 (2000).
13. C. Genies, R. Mercier, B. Sillion, N. Cornet, G. Gebel, and M. Pineri, *Polymer*, **42**, 359 (2001).
14. S. Besse, P. Capron, O. Diat, G. Gebel, F. Jousse, D. Marsacq, M. Pineri, C. Marestin, and R. Mercier, *J. New Mater. Electrochem. Syst.*, **5**, 109 (2002).
15. K. Miyatake, H. Zhou, H. Uchida, and M. Watanabe, *Chem. Commun.*, 368 (2003).
16. K. Miyakake, N. Asano, and M. Watanabe, *J. Polym. Sci., Part A: Polym. Chem.*, **41**, 3901 (2003).
17. K. Miyatake, H. Zhou, T. Matsuo, H. Uchida, and M. Watanabe, *Macromolecules*, **37**, 4961 (2004).
18. K. Miyatake, H. Zhou, and M. Watanabe, *Macromolecules*, **37**, 4956 (2004).
19. C. Lee, S. Sundar, J. Kwon, and H. Han, *J. Polym. Sci., Part A: Polym. Chem.*, **42**, 3612 (2004).
20. C. Lee, S. Sundar, J. Kwon, and H. Han, *J. Polym. Sci., Part A: Polym. Chem.*, **42**, 3621 (2004).
21. G. Gebel, L. Gonon, G. Meyer, and C. Perrot, 15th Annual Meeting of NAMS, Honolulu, Hawai, June 26–30, 2004.
22. G. Meyer, G. Gebel, L. Gonon, P. Capron, D. Marscaq, C. Marestin, and R. Mercier, *J. Power Sources*, (2006) in press.
23. J. Fang, X. Guo, S. Harada, T. Watari, K. Tanaka, H. Kita, and K. Okamoto, *Macromolecules*, **35**, 9022 (2002).
24. X. Guo, J. Fang, T. Watari, K. Tanaka, H. Kita, and K. Okamoto, *Macromolecules*, **35**, 6707 (2002).
25. K. Okamoto, *J. Photopolym. Sci. Technol.*, **16**, 247 (2003).
26. T. Watari, J. Fang, K. Tanaka, H. Kita, and K. Okamoto, *J. Membr. Sci.*, **230**, 111 (2004).
27. X. Guo, J. Fang, K. Tanaka, H. Kita, and K. Okamoto, *J. Polym. Sci., Part A: Polym. Chem.*, **42**, 1432 (2004).
28. X. Guo, J. Fang, and K. Okamoto, *Trans. Mater. Res. Soc. Jpn.*, **29**, 2579 (2004).
29. Y. Yin, S. Chen, X. Guo, J. Fang, K. Tanaka, H. Kita, and K. Okamoto, *High Perform. Polym.*, submitted.
30. B. R. Einsla, Y. S. Kim, M. A. Hickner, Y.-T. Hong, M. L. Hill, B. S. Pivovar, and J. E. McGrath, *J. Polym. Sci., Part A: Polym. Chem.*, **42**, 862 (2004).
31. B. R. Einsla, Y.-T. Hong, Y. S. Kim, F. Wang, N. Gunduz, and J. E. McGrath, *J. Membr. Sci.*, **255**, 141 (2005).
32. Y. Yin, J. Fang, Y. Cui, K. Tanaka, H. Kita, and K. Okamoto, *Polymer*, **44**, 4509 (2003).
33. Y. Yin, J. Fang, T. Watari, K. Tanaka, H. Kita, and K. Okamoto, *J. Mater. Chem.*, **14**, 1062 (2004).
34. Y. Yin, O. Yamada, Y. Suto, T. Mishima, K. Tanaka, H. Kita, and K. Okamoto, *J. Polym. Sci., Part A: Polym. Chem.*, **43**, 1545 (2005).
35. N. Asano, K. Miyatake, and M. Watanabe, *Chem. Mater.*, **16**, 2841 (2004).
36. J. Fang, X. Guo, and M. Litt, *Trans. Mater. Res. Soc. Jpn.*, **29**, 2541 (2004).
37. a) Y. Suto, Y. Yin, O. Yamada, K. Tanaka, H. Kita, and K. Okamoto, *Polym. Prepr., Jpn.*, **54**, 4605 (2005).
   b) Y. Suto, Y. Yin, O. Yamada, K. Tanaka, H. Kita, and K. Okamoto, *Macromolecules*, submitted.
38. Z. Hu, Y. Yin, S. Chen, K. Tanaka, H. Kita, and K. Okamoto, *J. Polym. Sci., Part A: Polym. Chem.*, submitted.
39. S. Chen, K. Tanaka, H. Kita, and K. Okamoto, *Polymer*, submitted.
40. Y. Yin, O. Yamada, H. Kita, and K. Okamoto, *Macromol. Rapid Commun.*, **26**, 696 (2005).
41. Y. Yin, Y. Suto, T. Sakabe, S. Chen, S. Hayashi, T. Mishima, O. Yamada, K. Tanaka, H. Kita, and K. Okamoto, *Macromolecules*, in press.
42. C. Genies, R. Mercier, B. Sillion, R. Petiaud, N. Cornet, G. Gebel, and M. Pineri, *Polymer*, **42**, 5097 (2001).
43. T. D. Gier, G. E. Munn, and F. C. Wilson, *J. Polym. Sci., Polym. Phys. Ed.*, **19**, 1687 (1981).
44. C. A. Edmondson and J. J. Fontanella, *Solid State Ionics*, **152–153**, 355 (2002).
45. W. Y. Hsu, J. R. Barkley, and P. Meakin, *Macromolecules*, **13**, 198 (1980).
46. T. Xu, W. Yang, and B. He, *Chem. Eng. Sci.*, **56**, 5343 (2001).
47. F. Lufrano, I. Gatto, P. Staiti, V. Antonucci, and E. Passalacqua, *Solid State Ionics*, **145**, 47 (2001).
48. N. Carretta, V. Tricoli, and F. Picchioni, *J. Membr. Sci.*, **166**, 189 (2000).
49. B. D. McNicol, D. A. J. Rand, and K. R. Williams, *J. Power Sources*, **83**, 15 (1999).
50. A. S. Arico, S. Srinivasan, and V. Antonucci, *Fuel Cells*, **1**,

133 (2001).
51. Z. Qi and A. Kaufman, *J. Power Sources*, **110**, 177 (2002).
52. V. Tricoli, N. Carretta, and M. Bartolozzi, *J. Electrochem. Soc.*, **147**, 1286 (2000).
53. X. Zhou, J. Weston, E. Chalkova, M. A. Hofmann, C. M. Ambler, H. R. Allcock, and S. N. Lvov, *Electrochim. Acta*, **48**, 2173 (2003).
54. Y. A. Elabd, E. Napadensky, J. M. Sloan, D. M. Crawford, and C. W. Walker, *J. Membr. Sci.*, **217**, 227 (2003).
55. J. Ding, C. Chuy, and S. Holdcroft, *Macromolecules*, **35**, 1348 (2002).
56. J. M. Bae, I. Honma, M. Murata, T. Yamamoto, M. Rikukawa, and N. Ogata, *Solid State Ionics*, **147**, 189 (2002).
57. Y. Woo, S. Y. Oh, Y. S. Kang, and B. Jung, *J. Membr. Sci.*, **220**, 31 (2003).
58. K. Okamoto, Y. Yin, O. Yamada, M. N. Islam, T. Honda, T. Mishima, Y. Suto, K. Tanaka, and H. Kita, *J. Membr. Sci.*, **258**, 115 (2005).
59. O. Yamada, Y. Yin, K. Tanaka, H. Kita, and K. Okamoto, *Electrochim. Acta*, **50**, 2655 (2005).
60. Y. Yin, O. Yamada, S. Hayashi, K. Tanaka, H. Kita, and K. Okamoto, *J. Polym. Sci., Part A: Polym. Chem.*, submitted.
61. a) O. Yamada, Y. Yin, T. Fukuda, K. Tanaka, H. Kita, and K. Okamoto, The 45th Battery Symposium in Japan, November 27–29, 2004.
b) O. Yamada, Y. Yin, T. Fukuda, K. Tanaka, H. Kita, and K. Okamoto, *J. Power Sources*, submitted.
62. L. Jorissen, V. Gogel, J. Kerres, and J. Garche, *J. Power Sources*, **105**, 267 (2002).
63. T. Yamaguchi, F. Miyata, and S. Nakao, *Adv. Mater.*, **15**, 1198 (2003).
64. V. S. Silva, B. Ruffmann, H. Silva, Y. A. Gallego, A. Mendes, L. M. Maderia, and S. P. Nunes, *J. Power Sources*, **140**, 34 (2005).
65. O. Yamada, T. Ogo, Y. Yin, K. Tanaka, H. Kita, and K. Okamoto, *Polym. Prepr., Jpn.*, **54**, 4535 (2005). To be submitted to *J. Power Sources*.
66. X. Ren and S. Gottesfeld, *J. Electrochem. Soc.*, **148**, A87 (2001).
67. Y. S. Kim, M. J. Summer, W. L. Harriso, J. S. Riffle, J. E. McGrath, and B. S. Pivovar, *J. Electrochem. Soc.*, **151**, A2150 (2004).
68. T. Yamaguchi, H. Kuroki, and F. Miyata, *Electrochem. Commun.*, **7**, 730 (2005).

Yan Yin was born in Hebei province, China in 1974. She received her master degree from Tianjin Polytechnic University, China, in 1999 and her Ph.D. in 2003 from Yamaguchi University under the direction of Prof. Ken-ichi Okamoto. Subsequently, she worked as a postdoctoral researcher in Prof. Okamoto's lab focused on the structure-morphology-property relationships of fuel cell membranes. Yin's current research interests include developing new membranes for polymer electrolyte fuel cells and direct methanol fuel cells.

Otoo Yamada was born in Munich, Germany in 1971. He received Ph.D. from Yamaguchi University in 2000 for studies on the positive electrode characteristics of lithiated metal oxides in organic electrolyte solutions. He joined Yamaguchi University Collaborative Research Center as a Research Associate. From 2002, he worked at Prof. Okamoto's lab as a post doctor on polymer electrolyte fuel cell. His current research interests include application of polymer electrolyte membranes for polymer electrolyte fuel cells and direct methanol fuel cells.

Kazuhiro Tanaka was born in Shiga, Japan in 1962. He received his B.S. and M.S. from Yamaguchi University and his Ph.D. from Osaka University. He joined the faculty of Yamaguchi University in 1988 and was promoted to Associate Professor in 1998. He worked as a visiting researcher at University of Colorado at Boulder in 1997–1998. His research interests are membranes for fuel cell and gas separation applications.

Ken-ichi Okamoto was born in 1941 in Hiroshima Prefecture, Japan. He received his M.S. Engineering from Osaka University in 1968. He joined Osaka University as a research associate. In 1971, he joined Yamaguchi University as an assistant professor. He received his Dr. Eng. from Osaka University in 1974. He joined Temple University as a visiting assistant professor for a year since August 1977. Since 1980, he has been in Yamaguchi University as a professor. He received Technology Award (2002) of The Society of Chemical Engineers Japan for development and industrial applications of zeolite membranes. His research focused on organic photoconductors, photocatalytic and photosensitized reactions, membrane separation materials and processes, and polymer electrolyte membranes and their fuel cell applications.